

~~CONFIDENTIAL~~

Copy
RM E50B02

34

NACA RM E50B02

E 50 B 02

TECH LIBRARY KAFB, NM
0143654

NACA

RESEARCH MEMORANDUM

CHARACTERISTICS OF PERFORATED DIFFUSERS

AT FREE-STREAM MACH NUMBER 1.90

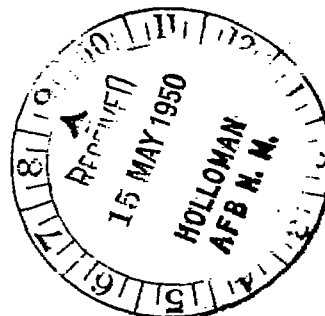
By Henry R. Hunczak and Emil J. Kremzier

Lewis Flight Propulsion Laboratory
Cleveland, Ohio

See 7th

CLASSIFIED DOCUMENT

~~CONFIDENTIAL~~
This document contains classified information
relating to the National Defense of the United
States within the meaning of the Espionage Act,
USC 50. It is to be controlled in such a manner
as to prevent unauthorized transmission or the
revelation of its contents in any manner to an
unauthorized person. It is to be controlled by law,
information so classified is to be reported
only to persons in the United States, and to
civilian officers and employees of the United States
Government who have a legitimate need to know
thereof, and to United States citizens of known
loyalty and discretion who of necessity must be
informed thereof.



**NATIONAL ADVISORY COMMITTEE
FOR AERONAUTICS**

WASHINGTON
May 8, 1950

~~CONFIDENTIAL~~

Classification cancelled (or changed to UNCLASSIFIED)

By Authority of NASA Tech Rep Announcement #46
(OFFICER AUTHORIZED TO CHANGE)

By 31 Nov 53
NAME AND

NMB
(GRADE OF OFFICER MAKING CHANGE)

12 Apr 61
DATE



NACA RM E50B02

NATIONAL ADVISORY COMMITTEE FOR AERONAUTICS

RESEARCH MEMORANDUM

CHARACTERISTICS OF PERFORATED DIFFUSERS

AT FREE-STREAM MACH NUMBER 1.90

By Henry R. Hunczak and Emil J. Kremzier

SUMMARY

An investigation of a series of perforated convergent-divergent diffusers was conducted in the NACA Lewis 18- by 18-inch tunnel at a Mach number of 1.90. Contraction ratios of 1.40, 1.49, 1.53, 1.55, 1.59, 1.63, and 1.70 and various perforation distributions were investigated to determine (a) the average subsonic flow coefficient (effective area ratio), (b) the perforation distribution required for establishing supersonic flow in the inlet, and (c) the effect of various perforation distributions on peak total-pressure recoveries, relative mass flow, and shock stability.

The circular, sharp-edged orifices used to perforate the inlets had an average subsonic flow coefficient of 0.5 when spilling the subsonic flow behind the normal shock.

A wide range of peak total-pressure recoveries and relative mass flows were obtained over the range of contraction ratios investigated. A maximum total-pressure recovery of 96 percent was obtained with an inlet having a contraction ratio of 1.63. The relative mass flow at this recovery was 82 percent. An inlet with a contraction ratio of 1.40 gave a maximum relative mass flow of 98 percent while attaining a total-pressure recovery of 0.90.

Pressure recoveries up to 92 percent were obtained using a theoretical distribution of perforations based on the design considerations for neutral shock equilibrium. For some of these configurations, shock stability at the throat of the inlet was observed. Additional perforations upstream of the throat stabilized the shock in the converging section of the diffuser and improved the pressure recovery, but reduced the relative mass flow.

Agreement between theoretical and experimental relative mass flows was within approximately 1 percent over a range of contraction ratios from 1.40 to 1.59 with the perforation distributions used.

INTRODUCTION

Supersonic diffusion that results in pressure recoveries exceeding those of a free-stream normal shock is usually obtained by decreasing the shock Mach number through a contraction of the supersonic flow-stream tube. Two methods of contracting the flow-stream tube are by external diffusion in which the flow is compressed by a projecting cone or wedge, and by internal diffusion in which a converging channel forces a compression of the flow.

When the second method is employed, at least two factors limit the full utilization of the diffusion process. First, the contraction of the converging channel (inlet) is limited by the subsonic mass flow behind the normal shock, which must pass through the minimum area (throat) when the shock is at the inlet entrance; and second, when the shock is in the vicinity of the minimum area or throat, its instability limits the minimum shock Mach number that can be realized (references 1 and 2).

Perforations along inlet walls may be utilized to minimize or to eliminate the contraction limitation and the shock instability discussed in the previous paragraph (reference 3). Because of the static-pressure rise across a normal shock, the perforations along the inlet spill a high rate of mass flow when the shock is ahead of the inlet and the static-pressure differential across the perforations is high, and spill a low rate of mass flow when the shock is at the throat and the static-pressure differential is low. (Thus the inlet can contract the flow until the shock occurs at sonic velocity and the static pressures before and after the shock are equal.) For positions of the shock in the inlet, the perforations tend to maintain a balance of the flow spillage necessary to stabilize the shock; therefore, with the normal shock occurring at sonic or close to sonic velocity and with shock stability, high pressure recoveries are obtained (reference 3).

An inherent characteristic of the perforated inlet is the continuous flow spillage through the perforations when the shock is at or downstream of the throat. Although spillage may represent a loss in thrust on a ram-jet configuration, it may also serve as a boundary-layer bleed and a source of flow turbulence to minimize flow separation.

A study was made at the NACA Lewis laboratory of some of the stability considerations of the perforated convergent-divergent diffuser. The pressure recoveries that can be obtained with

CONFIDENTIAL

perforated inlets over a range of contraction ratios and the amount of mass flow spilled associated with each inlet were experimentally determined. A method of evaluating the relative merits of increase in pressure recovery associated with this lost mass flow on an internal-thrust-coefficient basis is also included.

SYMBOLS

The following symbols are used in this report:

- A summation of perforated area upstream of diffuser throat, (sq ft)
- B $\left[\frac{\gamma}{RT} \left(\frac{2}{\gamma+1} \right)^{\frac{\gamma+1}{\gamma-1}} \right]^{\frac{1}{2}}$
- C_t internal thrust coefficient
- D diameter, (in.)
- F thrust, (lb)
- f fuel-air ratio
- g acceleration due to gravity, (ft/sec²)
- L length along inlet measured from entrance of supersonic inlet, (in.)
- M Mach number
- m mass flow, (slugs/sec)
- P stagnation or total pressure, (lb/sq ft)
- p static pressure, (lb/sq ft)
- Q_a subsonic flow coefficient of perforations (effective-area ratio)
- Q_b supersonic flow coefficient of perforations (effective-area ratio)
- q dynamic pressure, (lb/sq ft)
- R gas constant, (ft/°R)
- S diffuser area, (sq ft)

- T stagnation temperature, ($^{\circ}$ R)
- v velocity, (ft/sec)
- β angle between velocity vector v and outward-drawn vector normal to dA, (deg)
- γ ratio of specific heats
- θ angle between final Mach line and diffuser wall, (deg)
- ρ static density, (slugs/cu ft)
- τ heat-release parameter
- ϕ coordinate angle between Mach line at $M = 1$ and local Mach line, (deg)
- ψ Prandtl-Meyer expansion angle, (deg)
- ω angle between positive direction of x and outward-drawn vector normal to dA, (deg)

Subscripts:

- 0 free stream
- 1 inlet entrance
- 2 inlet throat
- 3 pitot-static rake in simulated combustion chamber
- 4 outlet of simulated combustion chamber or ram-jet exhaust nozzle
- e exit of perforations
- x,y local stations within diffuser
- * indicates conditions at sonic velocity

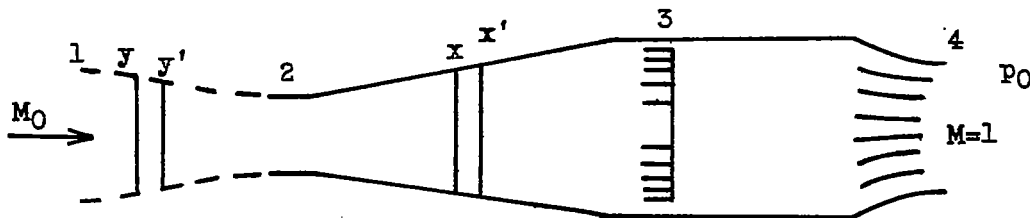
ANALYSIS

The characteristics of the perforated diffuser at a given free-stream Mach number may, in part, be controlled by the

contraction ratio and the distribution of perforations. The analysis to determine these characteristics is in three parts: (1) the criterion for stable, unstable, and neutral shock equilibrium in the convergent portion of the diffuser, (2) the design of diffusers for neutral shock equilibrium, and (3) the conditions for normal shock entrance. A knowledge of the concepts of reference 3 is assumed.

Criterion for stable, unstable, and neutral shock equilibrium. -

A normal shock is in stable equilibrium if momentary displacements of the shock are accompanied by reactions that tend to return the shock to its equilibrium position. Stability of the shock at various stations in the perforated diffuser shown in the following sketch may be determined by means of the equation of continuity assuming one-dimensional flow:



Regardless of the position of the shock, the mass flow through the throat of the diffuser (station 2) must equal the mass flow through the choked outlet (station 4); therefore

$$m_2 = m_4 = \frac{P_2 S_2 M_2}{\frac{\gamma+1}{2(\gamma-1)}} \sqrt{\frac{\gamma}{gRT_2}} = \frac{P_4 S_4}{\frac{\gamma+1}{2(\gamma-1)}} \sqrt{\frac{\gamma}{gRT_4}} \quad (1)$$

$$\left(1 + \frac{\gamma-1}{2} M_2^2\right) \quad \left(\frac{\gamma+1}{2}\right)$$

For the case of no heat addition, $\sqrt{\frac{\gamma}{gRT_2}} = \sqrt{\frac{\gamma}{gRT_4}}$ and if the shock is downstream of the throat, $P_2 S_2$ and M_2 are constant so that for shock equilibrium the product $P_4 S_4$ must be constant. Should the shock be displaced from its equilibrium position, from S_x to $S_{x'}$, by means of some temporary disturbance, the Mach number ahead of the shock will increase and hence P_4 will decrease. For a constant outlet area S_4 , insufficient mass flow will egress through the outlet, the shock will be moved towards its equilibrium position, and the condition will be stable.

When the shock is located upstream of the throat, the flow between the throat and the outlet is subsonic, the stagnation pressure P_4 can be considered proportional to P_2 in equation (1), and the throat Mach number M_2 is then a function of only the outlet area S_4 . Equation (1) is now satisfied for a range of values of the throat stagnation pressure.

If the equilibrium position of the shock is at S_y , the mass flow through the shock must equal the mass flow through the throat plus the mass flow through the perforations between S_y and S_2 . A transient displacement of the shock from S_y to S_y' will increase the throat stagnation pressure and hence will increase the mass flow through the throat and through the perforations between S_y' and S_2 . This increase and its counterpart, the decrease in mass flow through the perforations between S_y and S_y' , is expressed as a fraction of the mass flow through the shock station S_y' . For neutral shock equilibrium, the fractional increase in mass flow through the throat and perforations between S_y' and S_2 must be equal to the fractional decrease in mass flow through the perforations between S_y and S_y' . If stable equilibrium is to occur, the fractional decrease in mass flow through the perforations between S_y and S_y' must be greater than the fractionally increased mass flow through the throat and perforations between S_y' and S_2 . The air will then accumulate downstream of the shock and force it towards its equilibrium position. Similarly, unstable equilibrium will occur should the fractional decrease in mass flow through the perforations between S_y and S_y' be less than the fractional increase in mass flow through the throat and perforations between S_y' and S_2 . It should be noted that the criterion for shock equilibrium depends only on the local conditions. At any station along a given inlet the stability of the shock may therefore be made unstable, neutral, or stable by adjusting the distribution of the perforations.

The condition for shock stability may be alternately expressed in terms of the throat Mach number, the equilibrium position of the shock, and the outlet area S_4 . For neutral equilibrium, the required fractional change in mass flow through the diffuser throat must be proportional to the fractional change in total pressure behind the shock should the shock move from S_y to S_y' . The throat Mach number then remains constant, which satisfies equation (1) for a constant outlet area S_4 . For stable equilibrium, the

required mass flow through the diffuser throat must increase in greater proportion than the throat total pressure should the shock move from S_y to S_y' . The throat Mach number then tends to increase and equation (1) is satisfied only if the shock returns to S_y or the outlet area S_4 is increased.

Design of diffusers for neutral shock equilibrium. - The theoretical treatment of reference 3 presents a method of determining and correlating the perforation distribution A/S_{2*} and the local contraction ratio S/S_{2*} as a function of the local Mach number M to obtain a perforated isentropic inlet. With this type of inlet, the free-stream flow is decelerated to sonic velocity at the throat S_{2*} for any position of the normal shock between the inlet entrance S_1 and the throat. The local Mach number at any given station changes only when the shock moves past the station. Only two Mach numbers may therefore exist at a given station, either a supersonic Mach number or a subsonic Mach number that is related to the supersonic Mach number by the normal shock relations. Such diffusers give neutral shock equilibrium and have the minimum area of perforations to allow the supersonic flow to be established. The geometric contraction ratio S_1/S_{2*} of the inlet is greater than the isentropic contraction ratio S_1/S_* for the free-stream Mach number M_0 because of the flow spillage through the perforations after the shock has been swallowed.

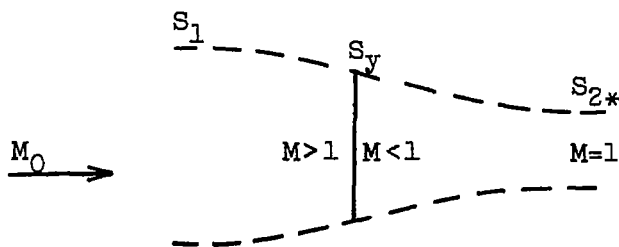
The following assumptions were made:

1. One-dimensional flow exists through the inlet.
2. A total-pressure loss in the inlet occurs only through the normal shock.
3. The subsonic flow coefficient is constant and the mass flow through the perforations downstream of the normal shock is choked and varies only with the total pressure.
4. The supersonic flow through the perforations may be described by Prandtl-Meyer two-dimensional theory.

The mathematical equations (from reference 3) used for calculations are given in appendix A along with a simplified method of obtaining desired quantities through the use of available supersonic flow tables (reference 4).

The theoretical curves for a perforated isentropic inlet are presented in figures 1 and 2. The calculations for these curves are based on a free-stream Mach number of 1.90 and the assumption that the static pressure at the exit of the perforations p_e is equal to the free-stream static pressure p_0 . These figures are plots of the summation of the ratio of perforated area to throat area A/S_{2*} and the ratio of diffuser area to throat area S/S_{2*} as functions of the local Mach number. Because of a lack of experimental data on flow coefficients for sharp-edged orifices having components of velocity normal and tangential to their surfaces, the calculations were made for constant subsonic flow coefficients Q_a of 0.4, 0.5, 0.6, and 0.7. Figures 1 and 2 may be used to obtain the relations of the ratios of perforated area and diffuser area to throat area required for neutral shock equilibrium for any inlet whose geometric contraction ratio S_1/S_2 is less than that of the perforated isentropic inlet from the following considerations:

A perforated isentropic inlet with the normal shock occurring at any local area (as shown in the following sketch) may be cut off at the local area S_y to obtain a new inlet whose contraction ratio S_1/S_2 is equal to the area ratio S_1/S_y . The perforation distribution is such that neutral shock equilibrium still exists for all positions of the normal shock between S_1 and S_y because the flow conditions upstream of and the mass flow immediately downstream of the normal shock are not changed.



The Mach number behind the normal shock at the new throat is now subsonic, but still remains constant for upstream displacements of the shock. In figures 1 and 2, dashed lines that represent constant values of the ratio of inlet-entrance area to diffuser area equal to the desired contraction ratio S_1/S_2 are shown. To the right of the dashed lines, the theoretical curves are applicable to the desired contraction ratios. The values of the ratios of perforated

area to throat area and diffuser area to throat area obtained from the theoretical curves, however, are in terms of the theoretical throat area S_{2*} and are displaced along the ordinate by the values corresponding to the part of the inlet that is no longer required.

Eliminating the local Mach number as the independent variable and converting the relations to a specific geometric contraction ratio results in a direct plot of the perforated-area to throat-area ratio as a function of the diffuser-area to throat-area ratio with the subsonic flow coefficient as an independent parameter, as shown in figure 3 for a contraction ratio of 1.55. (The contraction ratio for the perforated isentropic inlet is 1.675 at a flow coefficient of 0.5.) The curves determine the theoretical perforation distribution required for neutral shock equilibrium for each assumed value of the subsonic flow coefficient.

In the following discussions, reference is made to theoretical distribution, which is defined as a distribution of perforations giving neutral shock equilibrium for an assumed (constant) value of Q_a . Each curve in figure 3 is therefore theoretical according to definition; however, only the theoretical distributions corresponding to the true value of flow coefficient will provide neutral shock equilibrium in an actual inlet. The remaining theoretical curves may then be considered as variations of the perforation distribution from that required for the true subsonic flow coefficient and are given to illustrate the effect on shock equilibrium as the configuration is altered.

As an example, the true value of the subsonic flow coefficient is assumed to be 0.5. When the perforation distribution conforms to this value, the subsonic throat Mach number remains constant at 0.791 for all positions of the shock (the shock position is in terms of the ratio of inlet-entrance area to local diffuser area) within the inlet (fig. 4) and the equilibrium of the shock is neutral. Should the perforation distribution be increased to conform to that indicated by the subsonic flow coefficient of 0.4 while maintaining the true flow coefficient of 0.5, the throat Mach number increases continuously from 0.63 when the shock is at the inlet entrance to 0.77 when the shock is at the throat, as shown by the lower curve of figure 4. The equilibrium of the shock is now stable. Conversely, for a decrease in the perforation distribution to that corresponding to a flow coefficient of approximately 0.55 the throat Mach number decreases continuously from 0.93 to 0.80 as the shock moves downstream within the inlet, as shown by the upper curve of figure 4. For this distribution the equilibrium of the shock is unstable.

The slope of the perforation-distribution curve (fig. 3) is of particular interest because it is nearly constant and changes only with subsonic flow coefficient. The slope may therefore be considered independent of the absolute value of the local diffuser-area to throat-area ratio and the local shock Mach number. Consequently, by comparing the slope of the curve at local stations of an arbitrary perforation distribution (a variable slope) with that of the theoretical curve for the true value of the subsonic flow coefficient, the local regions of stable, unstable, and neutral shock equilibrium may be determined.

Conditions for normal shock entrance. - For inlets with contraction ratios less than that of the perforated isentropic inlet, the minimum ratio of total perforated area to throat area required to bring the shock to the inlet entrance with the throat choked is less than that required for neutral shock equilibrium. The relations for this minimum total-area ratio can be derived from the equation of continuity on a one-dimensional basis as

$$\left(\frac{A_1}{S_2}\right)_{\min} = \frac{1}{Q_a} \left[\frac{P_0}{P_2} \frac{S_1}{S_2} M_0 \left(\frac{\frac{\gamma+1}{2}}{1 + \frac{\gamma-1}{2} M_0^2} \right)^{\frac{\gamma+1}{2(\gamma-1)}} - 1 \right] \quad (2)$$

When the shock is at the inlet entrance, the throat velocity is sonic and the mass flow at the throat m_2 equals the mass flow entering the inlet entrance at free-stream conditions m_0 minus that through the perforations m_e . If the perforation distribution is such that the throat will not choke for any intermediate location of the shock between the entrance and the throat, the shock will be swallowed and supersonic flow will be established throughout the inlet. Such a distribution may be obtained by using a theoretical distribution (as defined in conjunction with fig. 3) corresponding to a subsonic flow coefficient greater than the true value such that the minimum total perforated area is the required amount.

The minimum ratio of total perforated area to throat area A_1/S_2 as a function of the geometric contraction ratio S_1/S_2 (dashed curve fig. 5) is compared with the ratio of total perforated area to throat area required for neutral shock equilibrium (solid curve) in figure 5 for a free-stream Mach number equal to 1.90 and subsonic flow coefficients of 0.4, 0.5, 0.6, and 0.7. The fact that no perforations are required to permit supersonic flow to be established through the inlet at a geometric contraction ratio of 1.193

is substantiated by the analytical and experimental data in reference 1. The two curves join when the geometric contraction ratio equals the perforated isentropic contraction ratio and the perforation distributions are then unique.

APPARATUS AND PROCEDURE

The investigation was conducted in the NACA Lewis 18- by 18-inch supersonic tunnel at a diffuser-inlet Mach number of 1.90 ± 0.01 . The stagnation temperature of the air was maintained at approximately 140°F with electric heaters and the dew point was reduced to -20°F with activated alumina air driers.

The investigation was made with a family of eight converging inlets, ranging in geometric contraction ratio S_1/S_2 from 1.40 to 1.70 and having equal throat areas. Internal contours of all inlets were designed on a one-dimensional basis by assuming the inlet-entrance Mach number to be the isentropic value corresponding to the geometric contraction ratio, and by assuming an almost linear reduction in local Mach number to sonic velocity in an axial length of 1.945 throat diameters. A throat length of 0.65 throat diameter was then added to aid shock stability. A schematic diagram of an inlet giving the principal dimensions and a table of coordinates for the various inlets investigated are shown in figure 6. The wall thickness of the inlets was approximately $3/32$ inch, which determined the external contours. A short cylindrical section of arbitrary length was added to the entrance of each inlet to facilitate the use of a sharp entrance edge and to establish the desired wall thickness ahead of the initial perforations.

The perforations in each inlet were initially drilled with a number 43 drill (0.089-in. diam.) perpendicular to the internal contour at axial stations $1/16$ inch apart. They were then made into sharp-edged orifices with a standard 82.5° countersink. At each station, the perforations were arbitrarily spaced around the circumference to produce as uniform an over-all density pattern as possible. The actual hole sizes were then measured. A half-section of an inlet shown in figure 7 illustrates a typical perforation pattern.

Modifications of the initial perforation distributions were made by either enlarging the existing holes on each inlet or by adding holes of the same diameter as the preceding perforations. Throughout the entire investigation, however, the average diameter of all holes drilled in any one inlet did not exceed 0.12 inch.

All inlets were mounted on the same test apparatus used in references 2 and 3. A schematic diagram of the 5° conical subsonic diffuser and simulated combustion chamber is shown in figure 8(a). The 90° conical outlet control was used to regulate the back pressure on the diffuser.

Pressure instrumentation consisted of a 40-tube pitot-static survey rake located 0.55 combustion-chamber diameter downstream of the outlet of the subsonic diffuser (fig. 8(b)). The rake was so designed that each pitot-static tube was located at the centroid of one of the forty equal area segments into which the combustion-chamber cross section was divided.

All pressure readings were taken on a multiple-tube differential manometer board with acetylene tetrabromide as a working fluid and were photographically recorded. Shock-wave configurations around the inlets were observed with a two-mirror schlieren system and photographs were taken of characteristic flow patterns.

Total-pressure recoveries were calculated by taking the numerical average of the total pressures measured with the pitot-static rake and dividing by the free-stream total pressure P_0 . Precision of measurements and calculations for pressure recovery was ± 0.2 percent for any particular run and ± 0.5 percent for the entire experimental program.

In order to evaluate the relative mass flows m_3/m_0 from the pitot-static pressures, the rake in the simulated combustion chamber was calibrated with three different unperforated inlets having known mass flows. A 5° diverging inlet, a cylindrical inlet, and a 5° converging inlet having a contraction ratio of 1.176 were used for the calibration. The mass flow entering the inlet entrance m_0 was calculated from the free-stream total pressure, Mach number, and inlet area on a one-dimensional basis. The mass flow m_3 through the combustion chamber was calculated by summing up the individual mass flows determined for each area segment from the corresponding pitot-static pressure ratio. Calculations at the combustion chamber were made on a one-dimensional basis, with a correction made for the area of the tubes in the rake. The calibrations gave a constant value of relative mass flow of 1.06 for all three inlets. This calibration factor was applied as a correction to all inlets investigated. From repeated test points, the precision of measurements of the relative mass flow m_3/m_0 was approximately $\pm 2\frac{1}{2}$ percent for a single

test point. For conditions when the relative mass flow remains constant as the total-pressure recovery varies, the precision is believed to be within ± 1 percent for an average of three or more test points.

Inlets with geometric contraction ratios less than 1.555 were used to determine the minimum ratio of total perforated area to throat area at which each inlet would swallow the normal shock. A high value of Q_a was first assumed and the inlet was perforated according to the corresponding theoretical distribution, as determined from figures 1 and 2 for the contraction ratio under consideration. The assumed value of Q_a was then incrementally decreased by adding perforations or by increasing the size of existing perforations until the shock was swallowed. The perforation distribution was maintained along a theoretical curve. In this manner, the experimental minimum ratio of total perforated area to throat area could be used in equation (2) to evaluate an average subsonic flow coefficient for the perforations. Comparisons of experimental data with the theoretical computations based on the experimental average subsonic flow coefficient could then be made. Perforations were then added near the throat to stabilize the shock for a short distance in the converging section, rather than along the entire inlet length, and to maintain the mass-flow loss in the supersonic region at a minimum. Further additions were made farther upstream to obtain the effect of stable shock equilibrium over a greater range of diffuser-area to throat-area ratios.

At the higher contraction ratios, the perforations near the throat required for shock stability were added to the initial perforations before the minimum ratio of total perforated area to throat area had been attained. The subsequent perforation distributions were again made to increase the range of stable shock equilibrium, as with the inlets of lower contraction ratio.

The perforation distributions used with the various inlets are shown in figure 9 and are designated by the letters a, b, c, and so forth. The summation of perforated-area to throat-area ratio A/S_2 is plotted as a function of diffuser-area to throat-area ratio S/S_2 . Perforation distributions designated "minimum for starting" conform to theory in that they were almost linear and were the first to allow complete entrance of the normal shock to the throats of the inlets. Those listed as "starting" allowed complete entrance of the normal shock but were not theoretical.

For identification, each configuration is designated by its geometric contraction ratio and perforation distribution. The two

inlets having a contraction ratio of 1.40 and identical contours are differentiated by the numerals 1 and 2. For comparison, the theoretical curve of neutral shock equilibrium for a subsonic flow coefficient of 0.5 is shown as a dashed line.

RESULTS AND DISCUSSION

Subsonic Flow Coefficient

The average subsonic flow coefficient calculated from the minimum ratios of total perforated area to throat area for starting in figure 9 and equation (2) was approximately 0.5, as graphically shown in figure 10. The minimum ratio of total perforated area to throat area as a function of the contraction ratio is compared with the theoretical curves from figure 5 for normal shock entrance and neutral shock equilibrium. Although the agreement between theory and experiment is good, any conclusion should be qualified by the fact that the subsonic flow coefficient thus obtained is an average value of all perforations in the inlet, and that the pressure differential is sufficient to cause the flow through the orifices to be choked. Any variation in the subsonic flow coefficient with the tangential or normal local Mach number is not apparent because each configuration covers the range of subsonic Mach numbers from 0.596 to 1.0 when the shock is at the inlet entrance.

Effect of Perforation Distribution

The configurations investigated may be grouped according to the theoretical consideration of the requirements for shock entrance into the inlets and shock equilibrium at the experimentally determined average subsonic flow coefficient of 0.5 into: (1) inlets having insufficient perforated area to permit normal shock entrance; (2) inlets having the minimum perforated area to permit normal shock entrance; (3) inlets with no region of stable shock equilibrium; and (4) inlets with some region of stable shock equilibrium. A further qualification necessary to differentiate between the configurations of the second and third groups is that those of the third group have more than the minimum perforated area required to permit normal shock entrance. Inlets with neutral shock equilibrium have been omitted because they form a borderline case between those of the third and fourth groups and it is doubtful that this condition of shock equilibrium could be experimentally obtained over the entire range of shock positions within the inlet.

Inlets having insufficient perforated area to permit normal shock entrance. - The total-pressure recovery P_3/P_0 as a

function of the relative mass flow $\frac{m_3}{m_0} = \frac{\rho_3 v_3 S_3}{\rho_0 v_0 S_1}$ was independent

of the perforation distribution and all curves remained similar (fig. 11). When the relative mass flow is variable (subcritical region of flow), the slight change in total-pressure recovery is largely the result of a change in subsonic diffusion losses because the only shock losses are external to the inlet entrance (reference 2). When the relative mass flow is small, the subsonic diffusion losses are negligible and the total-pressure recovery of 0.77 (fig. 11) corresponds to the total-pressure recovery across a free-stream normal shock (0.767).

At the transition from subcritical to supercritical flow (a constant relative mass flow), the throat Mach number reaches unity. The subsonic diffusion losses (without internal shocks) are then a maximum, and the total-pressure recovery of 0.74 is approximately constant for all the configurations listed in figure 11 and may be used to evaluate a subsonic diffuser pressure recovery P_3/P_2 of 0.74/0.77 or 0.96.

In the supercritical region of flow, the relative mass flow remains constant within the limits of precision of the instrumentation. The decrease in total-pressure recovery occurs through an internal shock because of an acceleration of the flow to supersonic velocities downstream of the throat (reference 2).

Configuration 1.63-b (fig. 11(k)) allowed a partial entrance of the normal shock into the inlet as a result of adding perforations near the inlet entrance. The peak pressure recovery of 0.815 is greater than the free-stream normal shock recovery of 0.770, and a discontinuity appears between the subcritical and supercritical conditions of flow.

The average relative mass flows of the supercritical flow conditions from figure 11 are presented in figure 12 with the geometric contraction ratio as the independent variable. The solid theoretical curve is given by the equation

$$\frac{m_3}{m_0} = \frac{m_2}{m_0} = \frac{P_2}{P_0} \frac{S_2}{S_1} \frac{M_2}{M_0} \left(\frac{1 + \frac{\gamma-1}{2} M_0^2}{1 + \frac{\gamma-1}{2} M_2^2} \right)^{\frac{\gamma+1}{2(\gamma-1)}} \quad (3)$$

~~CONFIDENTIAL~~

where P_2/P_0 is the pressure recovery through the free-stream normal shock ahead of the inlet entrance and the throat Mach number is unity.

The agreement between theoretical and experimental relative mass flows is within the precision of the instrumentation and verifies the assumption that the flow through the throat of the inlet may be considered one dimensional.

Inlets having minimum perforated area necessary to permit normal shock entrance. - Configurations with the minimum ratio of total perforated area to throat area $(A_1/S_2)_{\min}$ necessary to permit normal shock entrance have a large discontinuity between the subcritical and supercritical conditions of flow (fig. 13). The discontinuity in relative mass flow, which averaged approximately 20 percent, illustrates the relative effectiveness of the perforations in removing mass flow before and after the normal shock is swallowed. The curves of the subcritical conditions of flow remain unchanged, terminating at approximately the same end points. For supercritical flow conditions, the curves are displaced by the change in relative mass flow. The total-pressure recovery is increased through a reduction in shock Mach number. The relative mass flow remains constant up to the peak pressure recovery with no evidence of stable shock equilibrium within the inlet. The apparent increase in relative mass flow at low values of pressure recovery is probably due to measuring errors associated with the separations of the flow when the shock approaches the pitot-static rake.

The average experimental relative mass flow for the supercritical conditions of flow in figure 13 is shown in figure 14 and is compared with the theoretical values for normal shock equilibrium at a subsonic flow coefficient of 0.5. The average relative mass flow of each configuration is approximately $1\frac{1}{2}$ to 2 percent above the theoretical curve and is consistent with the theory and the experimentally determined value of the subsonic flow coefficient, because the perforated-area distribution in each case is less than that for normal shock equilibrium. The maximum relative mass flow of 0.98 for configuration 1.40-a-1 corresponds to the minimum ratio of total perforated area to throat area over the range of contraction ratios.

The theoretical data points in figure 14 were obtained by a numerical integration of the equation

~~CONFIDENTIAL~~

$$m_3 = m_2 = m_1 = \int_0^{A_1} \rho v Q_b dA \quad (4)$$

based on the theory of reference 3, in which the perforation distributions from figure 9 were used to evaluate dA in each case. The theoretical data show excellent agreement with the experimental results. Further comparisons in tabular form will be given subsequently.

Maximum total-pressure recoveries P_3/P_0 obtained with each configuration are shown in figure 15 for configurations with the minimum perforated-area distributions required for starting. The slight changes in peak pressure recovery (0.90 to about 0.91) are negligible compared to the range in contraction ratio from 1.40 to about 1.55. Because the normal shock was downstream of or at the throat of the inlet and the calculated reduction in throat Mach number with increasing contraction ratio for the configurations was from 1.42 to 1.25, the peak pressure recovery appears limited by either a decreasing effectiveness of the straight throat section in stabilizing the shock downstream of the throat (reference 2) or a deterioration of the subsonic diffusion process with increasing subsonic Mach number behind the shock. An appreciable gain in total-pressure recovery was obtained over the maximum of 0.838 reported in reference 2 for a convergent-divergent inlet with a contraction ratio of 1.176 at a Mach number of 1.85.

Inlets with unstable shock equilibrium. - Configurations with more than sufficient perforations to permit normal shock entrance but less than those required for neutral shock equilibrium had the same characteristics as those of the preceding group. (See fig. 16.) Although stable shock equilibrium was evidenced with configuration 1.49-d as a decrease in relative mass flow for positions of the shock within the inlet, the peak total-pressure recovery did not increase over that obtained with configuration 1.49-c (fig. 13). The stable shock equilibrium over the short range of relative mass flows was unexpected but was not surprising in view of the small deviation of the slope of the perforation-distribution curve from that of the theoretical curve. The maximum pressure recovery obtained was about 0.92 for configuration 1.53-d, which had a theoretical distribution of perforations based on the design considerations for neutral shock equilibrium.

Inlets with some region of stable shock equilibrium. - The relations of total-pressure recovery to relative mass flow are presented in figure 17 in an order of progressively increasing

~~CONFIDENTIAL~~

perforation distribution for each inlet (fig. 9). From these relations, stable shock equilibrium within the inlets may be noted as a continuous decrease in the relative mass flow from that of the supercritical condition of flow. Because the slopes of the perforation-distribution curves did not exceed the theoretical values required for neutral shock equilibrium over the entire range of diffuser-area to throat-area ratios, a discontinuity still exists but it is in the subcritical condition of flow, that is, the condition of variable relative mass flow.

The data points at total-pressure recoveries close to that of a free-stream normal shock correspond to the condition of a steady shock external to the inlet entrance. The second set of data points (for example, fig. 17(b)) in the subcritical condition of flow (below the peak pressure recoveries and above those of a free-stream normal shock) were obtained with only the more highly perforated configurations. These data points correspond to a condition of flow in which the normal shock rapidly oscillated from a position ahead of the inlet entrance to a position downstream of the diffuser throat. (The positions of the shock were observed from high-speed motion pictures of the schlieren image in which sections of the normal shock could be seen through perforations in alignment with the optical light path.) Because the pressure impulses were rapidly damped in the tubes between the pitot-static rake and the manometer, the pressure recoveries recorded are some average of the true pressure recoveries at the two extreme shock positions modified by the time the shock persists at each position. The relative mass flows are only a rough approximation because a prerequisite for the method of calculation used is a steady-state flow.

For configurations 1.49-g, 1.53-g, 1.55-e, 1.59-e, and 1.63-e (figs. 17 (i), (l), (o), (r), and (u), respectively), the oscillating type of flow extends over the entire subcritical region. The lower data points (a steady shock ahead of the inlet entrance) were obtained only when the tunnel was started with the diffuser outlet closed. According to theory, the shock should either remain in stable equilibrium within the inlet or revert to a corresponding position ahead of the inlet entrance. Whether the oscillating-flow phenomenon is an inherent characteristic of the perforated-type inlet, a characteristic of the test model, or an effect of local flow variations that may be remedied by using smaller, more numerous perforations is unknown.

The experimental results are in agreement with those theoretically expected from consideration of the effect of the slope of the perforation-distribution curve on stable shock equilibrium. With the

~~CONFIDENTIAL~~

exception of configuration 1.55-c (fig. 17(m)), all configurations indicate some stability. For configurations 1.40-c-1, 1.40-c-2, 1.53-e, 1.55-c, and 1.59-c, (figs. 17(a), (c), (j), (m), and (p), respectively), the slopes of the perforation-distribution curves exceeded those theoretically required for neutral shock equilibrium for only a short range of diffuser-area to throat-area ratios (approximately 1.05) and the degree of stable shock equilibrium is within the limits of instrumentation precision. As the slopes of the perforation-distribution curves were progressively increased over a greater range of local inlet-area ratios (approximately 1.20), the degree of stable shock equilibrium was increased.

The most significant discrepancy between the experimental results of figure 17 and the theory is the occurrence of the peak pressure recovery with the shock very close to its most upstream stable position within the inlet and the incremental increase in peak pressure recovery with perforation distribution after stable equilibrium of the shock has been obtained. Theoretical considerations of the inlet alone dictate that the peak pressure recovery be obtained when the shock Mach number is a minimum. This minimum shock Mach number is at the throat unless the increase in local Mach number due to the mass flow removed by the perforations $pvQ_b dA$ exceeds the decrease in local Mach number due to the contraction of the stream tube by the inlet wall. Thus, in terms of the perforation distribution slope, $\frac{dA/S_2}{dS/S_2} > \frac{1}{Q_b}$. The maximum peak

pressure recovery for a given contraction ratio, however, should be obtained with the first perforation distribution that allows stable shock equilibrium, because the minimum stable shock Mach number is the lowest. This discrepancy between theory and experiment cannot be rationalized within the limits of the assumptions made. Although the exact reasons for the increases in peak-pressure recovery are unknown, the occurrence may be the result of minimizing an interaction of the shock with boundary layer and of an improvement in subsonic-diffuser efficiency. Whereas the shock Mach number increases with the ratio of diffuser area to throat area, the perforations behind the shock provide a relief for any boundary-layer thickening caused by the adverse pressure gradient through the shock. The flow conditions at the entrance to the subsonic diffuser are thereby improved and a net improvement in peak pressure recovery could result. The limiting perforation distribution at which this effect produces the maximum peak pressure recovery for a given contraction ratio is not well defined. An increase in the perforation distribution slope over practically the entire length of configuration 1.59-e (fig. 9(f)), however, decreased the peak pressure recovery from approximately 0.95

to 0.94 (figs. 17(q) and 17(r)). A similar decrease in the peak pressure recovery is noted between configurations 1.70-a and 1.70-b (figs. 9(h), 17(v), and 17(w)).

At the contraction ratio of 1.40, the local increase in the slope of the perforation-distribution curve near the throat of the starting configuration 1.40-c-2 (fig. 9(b)) over that of 1.40-a-1 (fig. 9(a)) had no effect, and the same peak pressure recovery of 0.90 and relative mass flow of 0.98 were obtained. Also, the ratio of total perforated area to throat area required for starting was the same. At the higher contraction ratios of 1.59 and 1.63, the increase in the slopes of the perforation distributions improved the peak pressure recoveries for the starting configurations 1.59-c and 1.63-c (fig. 17(p) and (s), respectively) approximately 4 percent over the value of 0.90 for the starting configurations with theoretical perforation distributions (fig. 15). The starting ratios of total perforated area to throat area in figures 17(p) and (s) were increased above the values expected for a subsonic flow coefficient of 0.5 and the relative mass flows for supercritical conditions are approximately 2 percent below the theoretical values for neutral shock equilibrium given in figure 14.

The highest peak total-pressure recoveries at all contraction ratios were obtained with configurations highly perforated in the vicinity of the throat. The data points on figure 18 are for configurations 1.40-d-1, 1.40-f-2, 1.49-g, 1.53-g, 1.55-i, 1.59-d, 1.63-c, and 1.70-a. The solid curve is the theoretical peak pressure recovery for neutral shock equilibrium at a subsonic flow coefficient for the perforations of 0.5, and represents only normal shock losses at the inlet throat. The trend of the experimental data approximates the theoretical curve up to a contraction ratio of 1.55 and then levels off. Although the maximum experimental total-pressure recovery of 0.958 was obtained at a contraction ratio of 1.63, the experimental data have no well-defined peak, and pressure recoveries of approximately 0.95 were attained over a range of contraction ratios from 1.53 to 1.70.

Up to a contraction ratio of 1.55 the assumption of isentropic flow upstream of the shock is a good approximation at the Mach number of the investigation because the difference of approximately 3 percent between the highest peak total-pressure recoveries and the theoretical curve may be accounted for by the subsonic diffusion losses. At contraction ratios greater than 1.55, the experimental curve in figure 18 levels off at a value of approximately 5 percent below the theoretical values. This leveling off of the experimental curve may be the result of supersonic-diffusion losses, and at a

contraction ratio of 1.70 the supersonic diffusion losses may be estimated at approximately 2 percent if the subsonic diffusion losses are assumed constant.

The relative mass flows corresponding to the peak total-pressure recoveries presented in figure 18 were considerably below the theoretical values for neutral shock equilibrium. For configuration 1.63-e, (fig. 17(u)), the relative mass flow of 0.82 associated with the peak total-pressure recovery of 0.958 is approximately 12 percent less than the theoretical value. Calculations indicate that approximately 5 percent of this reduction is due to the increase in perforation distribution over the theoretical distribution; the remaining 7 percent is due to the increased flow spillage of perforations behind the normal shock in the converging portion of the inlet.

Comparison of Experimental and Integrated

Relative Mass Flows

The relative mass flow for supercritical conditions of operation may be evaluated by a numerical integration of equation (4). Experimental and integrated relative mass flows for supercritical flow conditions were compared. The results for several perforation distributions of the 1.49, 1.53, and 1.59 inlets are shown in the following table; the percentage variation is shown as positive when the integrated value exceeds the experimental value:

| Configuration | Mass-flow ratio, m_3/m_1 | | Variation (percent) |
|---------------|----------------------------|------------|------------------------|
| | Experimental | Integrated | |
| 1.49-c | 0.972 | 0.965 | -0.7 |
| 1.49-e | .956 | .949 | -.7 |
| 1.49-g | .934 | .922 | -1.3 |
| 1.53-c | 0.960 | 0.956 | -0.4 |
| 1.53-e | .942 | .938 | -.4 |
| 1.53-f | .931 | .924 | -.7 |
| 1.53-g | .906 | .896 | -1.1 |
| 1.59-c | 0.915 | 0.925 | 1.1 |
| 1.59-d | .901 | .910 | 1.0 |
| 1.59-e | .892 | .899 | .8 |

The variation between measured and integrated values remains approximately within the limits of experimental precision (± 1.0 percent). This agreement indicates that the proposed assumption and

~~CONFIDENTIAL~~

method of evaluating $\int_0^{A_1} \rho v Q_p dA$ in reference 3 give results that are practicable approximations to the supersonic flow through the perforations.

Visual Flow Observations

Typical schlieren photographs of the flow pattern about inlets with stable shock equilibrium are presented in figure 19 for several operating conditions. In figure 19(a) with the shock downstream of the throat, the mass flow spilled through the perforations is a minimum for the configuration, and is indicated qualitatively by the boundary layer that appears as a light area (upper half) and a dark area (lower half) adjacent to the inlet wall. With the shock positioned in the inlet, the increase in flow spillage is noticeable in figure 19(b) as a thickening of the light and dark areas downstream of the shock. (The approximate position of the internal shock is indicated by the arrow.) Coincident with this thickening, a flow compression emanates from the boundary layer. This compression is probably the result of a supersonic flow deflection generated by the increased flow spillage that appears to form the boundary layer into a virtual ramp. The transition in flow pattern between figures 19(a) and 19(b) was observed to be a continuous function of the shock position.

The appearance of the oscillating flow when visually observed is illustrated in figure 19(c). The range of shock positions was from the blurred image of the bow wave ahead of the inlet to a location downstream of the throat. Photographs taken at 4-microsecond exposure (figs. 19(d) and 19(e)) reveal the details of the shock pattern for two positions in its oscillation. In figure 19(d) the shock appears as a typical bow wave encountered in the subcritical condition of flow. The flow pattern behind the shock indicates considerable turbulence. In figure 19(e), the shock is within the inlet at a position coinciding approximately with the oblique wave emanating from the inlet wall. The flow is entering the inlet entrance at free-stream conditions and the shock pattern approximates that which would be expected under a steady-state flow condition.

Four-microsecond photographs of the inlet with the shock at its most downstream position of oscillation are unavailable. A study of high-speed motion pictures, however, indicates the flow pattern to be similar to that of figure 19(a).

~~CONFIDENTIAL~~

Angle of Attack

At an angle of attack of 3.9° , the highest peak pressure recoveries of figure 18 were reduced from 2 to 3 percent. In this respect, the performance of the inlets appears comparable to that of shock-type inlets. The change in relative mass flows from those obtained at zero angle of attack indicated slight reduction within the limits of instrumentation.

Estimation of Importance of Total-Pressure

Recovery and Relative Mass Flow

A method by which the relative merits of an increase in total-pressure recovery obtained at the expense of a decrease in relative mass flow may be evaluated is to determine the internal thrust coefficient $C_{t,3}$ for a simulated ram-jet unit from the experimental relations of total-pressure recovery to relative mass flow. The equation for the internal thrust coefficient as developed in appendix B is

$$C_{t,3} = \frac{0.525}{\frac{m_3}{m_0}} \frac{P_3}{P_0} \left[\frac{m_3}{m_0} \left(4.324 - 0.509 \frac{P_0}{P_3} \right) - 2 + 2 \left(1 - \frac{m_3}{m_0} \right) \frac{v_e}{v_0} \right] \quad (5)$$

In equation (5), the geometry of the ram-jet unit is variable so that the internal thrust coefficient is independent of physical dimensions. The velocity recovery v_e/v_0 represents the fraction of free-stream velocity retained by the air spilled through the perforations and is a design parameter as yet unknown. An inspection of equation (5) reveals, however, that should the velocity recovery equal unity the internal thrust coefficient has its limiting maximum value. No penalty is placed on the inlet for decreases in relative mass flow; identical results are obtained when the relative mass flow is unity. When the velocity recovery is zero, the reduction in internal thrust coefficient is a maximum; the internal thrust coefficient then has its limiting minimum values. In general, the velocity recovery should lie between unity and zero. Although variations in the velocity recovery with contraction ratio, perforation distribution, and relative mass flow may be expected, a first approximation may be made by holding the velocity recovery constant.

Typical internal thrust coefficients calculated from experimental values of total-pressure recovery and relative mass flow are presented in figures 20(a) and 20(b) for velocity recoveries of 0 and 0.6, respectively. The inlet contraction ratio is 1.49. Configurations with less than the minimum ratio of total perforated area to throat area required for starting and the subcritical conditions of flow with external shocks are not considered because they do not represent practicable design points. The dashed curves are lines of constant relative mass flow. A vertical displacement of a given data point below the dashed curve on which relative mass flow equals unity represents the change in internal thrust coefficient due to a momentum loss of spilled air.

The supercritical region of flow is indicated in figures 20(a) and 20(b) by the linear variation in internal thrust coefficient with total-pressure recovery. Shock stability in the converging section of the inlets is characterized by the decreasing slopes of the curves as the peak pressure recovery is approached.

When a velocity recovery of zero was assumed (fig. 20(a)), the effect of the momentum loss of the spilled air was severe. Configuration 1.49-c, which had the highest relative mass flow of 0.97 for its contraction ratio, gave the highest internal thrust coefficient of 0.814. Subsequent configurations 1.49-f and 1.49-g increased the peak total-pressure recoveries to 0.924 and 0.940 and reduced the internal thrust coefficient to 0.80 and 0.69, respectively. The peak internal thrust coefficients for all configurations corresponded closely to the supercritical conditions of flow.

For an assumed velocity recovery of 0.6, (fig. 20(b)), an increase in the peak internal thrust coefficient from 0.83 with configuration 1.49-c to approximately 0.84 for configuration 1.49-f was realized. The peak internal thrust coefficient of 0.823 for configuration 1.49-g is lower, but is in the subcritical region of flow.

At an assumed velocity recovery of unity, the highest internal thrust coefficients occur at the highest peak pressure recoveries. A value of internal thrust coefficient of 0.88 for configuration 1.49-g is obtained by vertically projecting the peak total-pressure recovery of 0.94 to the relative mass-flow curve of unity on either figure 20(a) or 20(b). Although this velocity recovery would not be encountered in practice, it represents a limiting condition of flow.

Over the entire range of contraction ratios and perforation distributions investigated, the highest values of the internal

thrust coefficients are presented in figure 21 for velocity recoveries of 0, 0.6, and 1.0. The configurations for these data points are listed in the following table:

| Inlet contraction ratio | Perforation distribution | | |
|-------------------------|--------------------------|-----|-----|
| | Velocity recovery | | |
| | 0 | 0.6 | 1.0 |
| 1.40-1 | a | c | d |
| 1.40-2 | c | d | f |
| 1.49 | c | f | g |
| 1.53 | e | e | g |
| 1.55 | d | f | h |
| 1.59 | c | c | d |
| 1.63 | c | c | e |
| 1.70 | a | a | a |

For an improvement in velocity recovery, the peak internal thrust coefficient appears to occur at higher contraction ratios and increased perforation distributions as indicated by figure 21 and the preceding table, respectively.

At an assumed velocity recovery of 0, the highest internal thrust coefficients are obtained between contraction ratios of 1.40 and 1.49. An increase in the velocity recovery to 0.6 shifts the highest internal thrust coefficient to a contraction ratio of approximately 1.59. For the limiting condition of velocity recovery equals 1.0, a contraction ratio of 1.63 that gives the maximum pressure recovery has the maximum internal thrust coefficient of 0.90.

In terms of perforation distributions the trend is similar. In general, configurations that first permitted normal shock entrance gave the highest values of peak internal thrust coefficient at a velocity recovery of zero. These configurations have the highest relative mass flow at their respective contraction ratios. (The one exception is configuration 1.53-e.) The data points correspond closely to the peak total-pressure recovery and to supercritical conditions of flow. At a velocity recovery of 0.6, the data points correspond to configurations with ratios of total perforated area to throat area greater than that required for normal shock entrance. All data points correspond to supercritical conditions of flow, but are not necessarily for the peak total-pressure recoveries of their respective configurations. For the limiting condition of velocity recovery equals 1.0, the data points correspond to the more highly perforated configuration at each contraction ratio. All data points are in the subcritical condition of flow and are for the peak total-pressure recovery.

A comparison may be made of the internal thrust coefficients of perforated inlets with the convergent-divergent inlets of reference 2 because the relative mass flow of the convergent-divergent inlets is unity. The values of internal thrust coefficient then coincide with the corresponding theoretical curve of figures 20(a) or 20(b). The inlet of 10° straight taper and 1.176 contraction ratio with a 2-inch cylindrical throat of reference 2 at a free-stream Mach number of 1.90 gave a peak total-pressure recovery of 0.810. The peak internal thrust coefficient for this inlet is 0.72, a decline of approximately 11 percent from the value of 0.814 for an inlet having a 1.49 contraction ratio at a velocity recovery of 0, and a reduction of approximately 15 percent from the value of 0.85 for an inlet having a contraction ratio of 1.59 at a velocity recovery of 0.6.

SUMMARY OF RESULTS

An investigation of perforated-type convergent-divergent inlets at a Mach number of 1.90 gave the following results:

1. The experimental average subsonic flow coefficient for the circular sharp-edged perforations used was approximately 0.50.
2. A maximum total-pressure recovery of 96 percent of the free-stream total pressure at a relative mass flow of 82 percent was obtained with an inlet having a contraction ratio of 1.63. A maximum relative mass flow of 98 percent was obtained with a peak pressure recovery of 90 percent using an inlet having a contraction ratio of 1.40.
3. Pressure recoveries up to 92 percent were obtained using a theoretical distribution of perforations based on the design considerations for neutral shock equilibrium. For some of these configurations, shock stability at the throat of the inlet was observed. Additional perforations upstream of the throat stabilized the shock in the converging section of the diffuser and improved the pressure recovery, but reduced the relative mass flow.
4. Theoretical (integrated) and experimental values of the supersonic flow removed by the perforations during supercritical operation agreed to approximately 1 percent over a range of contraction ratios from 1.40 to 1.59 and the perforation distributions investigated.
5. A theoretical comparison of the effectiveness of total-pressure recovery and relative mass flow was made in terms of an

internal thrust coefficient. For a velocity recovery of 0 of the flow spilled through the perforations, gains in pressure recovery were offset by losses in mass flow, and an inlet with a contraction ratio of 1.40 or 1.49 was found to be preferable. For a velocity recovery of 0.6, moderate mass-flow losses may be tolerated and an inlet with a contraction ratio of 1.59 gave the maximum internal thrust coefficient.

6. The maximum thrust coefficient of the perforated diffuser at a velocity recovery of zero was 11 percent greater than that of a convergent-divergent diffuser. At a velocity recovery of 0.6, the maximum internal thrust coefficient was 15 percent greater than that of a convergent-divergent diffuser.

Lewis Flight Propulsion Laboratory,
National Advisory Committee for Aeronautics,
Cleveland, Ohio.

~~CONFIDENTIAL~~

APPENDIX A

THEORETICAL EQUATIONS USED IN DESIGNING

PERFORATED INLETS

1254

The original derivation of the equation for calculating perforation size and distribution is given in reference 3. The calculations for $\frac{\rho v Q_b}{BP Q_a}$ and $\frac{\rho v}{\rho_e v_e} Q_b$ may be simplified if the equations are presented in a form that utilizes one-dimensional supersonic flow and normal shock relations, and two-dimensional Prandtl-Meyer expansion equations. These are available in tabulated form in reference 4.

The general equation that is numerically integrated to obtain the number and the distribution of perforations along a diffuser as a function of the local Mach number is

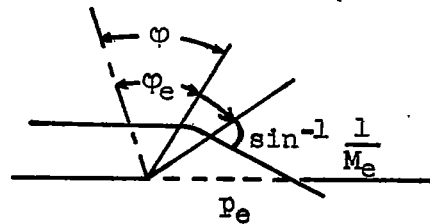
$$\left(\frac{A}{S_2}\right)_* = \frac{1}{Q_a} \left(\int_{M_*}^{M_1} \frac{\frac{1}{F} \frac{dP}{dM} dM}{1 - \frac{\rho v Q_b}{BP_2 Q_a}} - 1 \right) \quad (A1)$$

where

$$\frac{\rho v Q_b}{BP_2 Q_a} = \frac{1}{Q_a} \left(\frac{P_0}{P_2}\right) M_e \left(\frac{\frac{\gamma+1}{2}}{1 + \frac{\gamma-1}{2} M_e^2} \right)^{\frac{\gamma+1}{2(\gamma-1)}} \sin \left(\sin^{-1} \frac{1}{M_e} - \theta \right) \quad (A2)$$

and where M_e is obtained from the ratio of the static to total pressure p_e/P_0 and θ is the angle between the final Mach line and the diffuser wall.

~~CONFIDENTIAL~~



In terms of the coordinate angles φ and φ_e ,

$$\sin^{-1} \frac{1}{M_e} - \theta = \sin^{-1} \frac{1}{M_e} - \sin^{-1} \frac{1}{M} + (\varphi_e - \varphi) \quad (A3)$$

The coordinate angles may be expressed, however, in terms of the Prandtl-Meyer expansion angle ψ through which a stream must turn to expand from sonic velocity M_* to a supersonic Mach number M . Because

$$\varphi = \sqrt{\frac{\gamma+1}{\gamma-1}} \tan^{-1} \sqrt{\frac{\gamma-1}{\gamma+1}} (M^2 - 1)$$

and

$$\psi = \sqrt{\frac{\gamma+1}{\gamma-1}} \tan^{-1} \sqrt{\frac{\gamma-1}{\gamma+1}} (M^2 - 1) - \left(90 - \sin^{-1} \frac{1}{M} \right)$$

$$\sin^{-1} \frac{1}{M_e} - \theta = \psi_e - \psi \quad (A4)$$

The equation that is numerically solved in conjunction with equation (A1) to obtain the diffuser cross-sectional area as a function of the local Mach number is

$$\frac{S}{S_{2*}} = \frac{(\rho v)_*}{\rho v} + \frac{1}{\rho v} \int_0^A \rho v Q_b d \left(\frac{A}{S_{2*}} \right) \quad (A5)$$

Multiplying through by $\frac{\rho_e v_e}{\rho_e v_e}$ and $\frac{\rho_0 v_0}{\rho_0 v_0}$ gives

$$\frac{S}{S_{2*}} = \frac{\rho_0 v_0}{\rho v} \left[\frac{(\rho v)_*}{\rho_0 v_0} + \int_0^A \left(\frac{\rho v}{\rho_e v_e} Q_b \right) \frac{\rho_e v_e}{\rho_0 v_0} d \left(\frac{A}{S_{2*}} \right) \right] \quad (A6)$$

However,

$$\left. \begin{aligned} Q_b &= \frac{M_e}{M} \left(\frac{1 + \frac{\gamma-1}{2} M^2}{1 + \frac{\gamma-1}{2} M_e^2} \right)^{\frac{\gamma+1}{2(\gamma-1)}} \sin (\psi_e - \psi) \\ &= \frac{\rho_e v_e}{\rho v} \sin (\psi_e - \psi) \end{aligned} \right\} \quad (A7)$$

or

$$\frac{\rho v}{\rho_e v_e} Q_b = \sin (\psi_e - \psi) \quad (A8)$$

Also,

$$d \frac{A}{S_{2*}} = - \left(\frac{A}{S_{2*}} + \frac{1}{Q_a} \right) \frac{\frac{1}{P} \frac{dP}{dM} dM}{1 - \frac{\rho v Q_b}{B P_2 Q_a}} \quad (A9)$$

The quantities on the right side of equation (A9) have been previously calculated in evaluating equation (A1).

If the pressure p_e is assumed constant and equal to p_0 , $M_e = M_0$ in equations (A2), (A3), and (A4); and $\psi_e = \psi_0$ in equations (A4), (A7), and (A8).

It has been brought to the attention of the authors that a limiting condition for determining the exit Mach number M_e exists. When the final Mach line of the Prandtl-Meyer expansion at a perforation becomes parallel to the inlet wall, the angle θ in equations (A2), (A3), and (A4) is then zero and the exit Mach number a maximum. Should the final Mach line fall outside the inlet wall, the maximum exit Mach number $M_{e,max}$ of the perforation is the value that exists in the expansion at the Mach line that is parallel to the inlet wall; $M_{e,max}$ then becomes a function of only the local inlet Mach number and is given in terms of the Prandtl-Meyer expansion angle ψ by the equation

$$\psi = (\psi_e)_{max} - \sin^{-1} \frac{1}{M_{e,max}} \quad (A10)$$

A solution of equation (A10) for the maximum exit Mach number in terms of the local Mach number is shown in figure 22. These values for $M_{e,max}$ from figure 22 should be used to evaluate equations (A2), (A3), (A4), (A6), (A7), and (A8) whenever the final Mach line falls outside the inlet wall. For the assumption that the static pressure p_e is constant and equal to p_0 , this phenomenon first occurs at a local inlet Mach number of unity when the free-stream Mach number is 2.083.

APPENDIX B

BASIS FOR COMPARING DIFFUSERS TO DETERMINE

OPTIMUM DESIGN POINTS

The equation used to evaluate the design thrust coefficients shown in figure 20 was obtained through an integration of the momentum equation about a general ram-jet unit, considering only the effects of pressure recovery and relative mass flow of the air approaching the supersonic diffuser inlet. In order to isolate these internal effects, the external velocity is considered to be zero and the external pressure is assumed equal to the free-stream static pressure p_0 , which is analogous to having the air supplied to the unit at the free-stream Mach number M_0 by means of a ram pipe with a diameter equal to that of the diffuser inlet (fig. 23).

Integrating about the two-dimensional boundaries a, b, c, and d, the general equation for thrust is

$$F = \oint_{c \rightarrow d} p dA \cos \omega + \oint_{c \rightarrow d} (\rho v dA \cos \beta) v_x \quad (B1)$$

where the thrust is positive in the negative direction of x , ω is the angle between the positive direction of x and the outward-drawn vector normal to dA , and β is the angle between the velocity vector v and the outward-drawn vector normal to dA .

Across boundary \overline{ab} the mass flow m_0 emerging from the ram pipe may be segregated into three parts m_A , m_e , and m_2 for purposes of analysis. (m_A is the flow spilled ahead of the inlet entrance when the normal shock is upstream of station 1; m_e is the flow spilled through the perforations; and m_2 is the flow passing through the throat.) Across boundary \overline{cd} , the velocity of m_A and m_e is assumed to be v_A and v_e normal to \overline{cd} and at the free-stream static pressure p_0 . The mass flow m_4 issuing from the jet is choked and at a static pressure p_4 .

Integrating equation (B1), the internal thrust becomes

$$F = m_4 v_4 - m_0 v_0 + S_4(p_4 - p_0) + m_a v_a + m_e v_e \quad (B2)$$

The internal thrust coefficient based on the maximum area of the unit is

$$C_{t,3} = \frac{F}{q_0 S_3}$$

or, using one-dimensional and thermodynamic relations,

$$C_{t,3} = \frac{S_1}{S_3} \left[\frac{2 \frac{m_3}{m_0} (1+f)}{M_0} \sqrt{\tau} \left(\frac{1 + \frac{\gamma_0 - 1}{2} M_0^2}{\frac{\gamma_4 + 1}{2}} \right)^{\frac{1}{2}} \left\{ 1 + \frac{1}{\gamma_4} \left[1 - \frac{p_0}{p_4} \frac{\left(1 + \frac{\gamma_0 - 1}{2} M_0^2 \right)^{-\frac{\gamma_0}{\gamma_0 - 1}}}{\left(\frac{\gamma_4 + 1}{2} \right)^{-\frac{\gamma_4}{\gamma_4 - 1}}} \right] \right\}^{-2} + \frac{m_a v_a + m_e v_e}{q_0 S_3} \right] \quad (B3)$$

where the heat-release parameter is $\tau = \frac{\gamma_4 R_4 T_4}{\gamma_0 R_0 T_0}$, the relative mass flow is m_3/m_0 , and the fuel-air ratio is f .

For conditions where the normal shock is within the inlet entrance, m_A is zero. Then

$$\frac{m_e v_e}{q_0 S_3} = \frac{1 - \frac{m_3}{m_0} m_0 v_e}{q_0 S_3} = 2 \left(1 - \frac{m_3}{m_0} \right) \frac{v_e}{v_0} \frac{S_1}{S_3} \quad (B4)$$

S_1/S_3 may also be expressed as

$$\frac{S_1}{S_3} = \frac{\frac{1}{m_3} \frac{P_3}{P_0} \frac{M_3}{M_0} \left(\frac{1 + \frac{\gamma_0 - 1}{2} M_0^2}{1 + \frac{\gamma_0 - 1}{2} M_3^2} \right)^{\frac{\gamma_0 + 1}{2(\gamma_0 - 1)}}}{\frac{m_3}{m_0}} \quad (B5)$$

when γ equals γ_0 .

The thrust coefficient then becomes

$$C_{t,3} = \frac{\frac{1}{m_3} \frac{P_3}{P_0} \frac{M_3}{M_0} \left(\frac{1 + \frac{\gamma_0 - 1}{2} M_0^2}{1 + \frac{\gamma_0 - 1}{2} M_3^2} \right)^{\frac{\gamma_0 + 1}{2(\gamma_0 - 1)}}}{\frac{m_3}{m_0}} \left[\frac{2 \frac{m_3}{m_0} (1+f)}{M_0} \sqrt{\gamma} \left(\frac{1 + \frac{\gamma_0 - 1}{2} M_0^2}{\frac{\gamma_4 + 1}{2}} \right)^{\frac{1}{2}} \right. \\ \left. \left\{ 1 + \frac{1}{\gamma_4} \left[1 - \frac{P_0}{P_4} \frac{\left(1 + \frac{\gamma_0 - 1}{2} M_0^2 \right)^{-\frac{\gamma_0}{\gamma_0 - 1}}}{\left(\frac{\gamma_4 + 1}{2} \right)^{-\frac{\gamma_4}{\gamma_4 - 1}}} \right] \right\} - 2 + 2 \left(1 - \frac{m_3}{m} \right) \frac{v_e}{v_0} \right] \quad (B6)$$

If the Mach number M_3 is held constant at 0.2 and the heat-release parameter at 4.0, the fuel-air ratio required will depend on the efficiency of the combustion process for a given fuel. For purposes

of comparison, however, the fuel-air ratio term may be neglected, γ_4 may be taken at 1.4, and the total pressure before and after combustion may be assumed equal with negligible change in the relative values of the thrust coefficient between the various inlets. From an evaluation of the constants in equation (B6) on this basis,

$$C_{t,3} = \frac{0.525}{\frac{m_3}{m_0}} \frac{P_3}{P_0} \left[\frac{m_3}{m_0} \left(4.324 - 0.5088 \frac{P_0}{P_3} \right) - 2 + 2 \left(1 - \frac{m_3}{m_0} \right) \frac{v_e}{v_0} \right] \quad (B7)$$

The lower limit of the total-pressure recovery P_3/P_0 for which equation (B7) is valid is obtained when $\frac{P_4}{P_3} = \frac{P_0}{P_3} = 0.528$, the static total-pressure ratio required for sonic velocity at the jet outlet. The lowest value of the relative mass flow for which the combustion chamber is the major diameter is given by

$$\frac{S_1}{S_3} = 1 = \frac{0.525}{\frac{m_3}{m_0}} \frac{P_3}{P_0}$$

or

$$\frac{m_3}{m_0} = 0.525$$

when

$$\frac{P_3}{P_0} = 1.0$$

Should the relative mass flow be less than the value thus determined, the inlet becomes the major diameter of the unit. It is noted that the internal thrust coefficient thus computed represents the design condition of a unit for the inlet test point considered.

~~CONFIDENTIAL~~

NACA RM E50B02

REFERENCES

1. Kantrowitz, Arthur, and Donaldson, Coleman duP.: Preliminary Investigation of Supersonic Diffusers. NACA ACR L5D20, 1945.
2. Wyatt, DeMarquis D., and Hunczak, Henry R.: An Investigation of Convergent-Divergent Diffusers at Mach Number 1.85. NACA RM E6K21, 1947.
3. Evvard, John C., and Blakey, John W.: The Use of Perforated Inlets for Efficient Supersonic Diffusion. NACA RM E7C26, 1947.
4. The Staff of the Ames 1- by 3-Foot Supersonic Wind-Tunnel Section: Notes and Tables for Use in the Analysis of Supersonic Flow. NACA TN 1428, 1947.

1254

~~CONFIDENTIAL~~

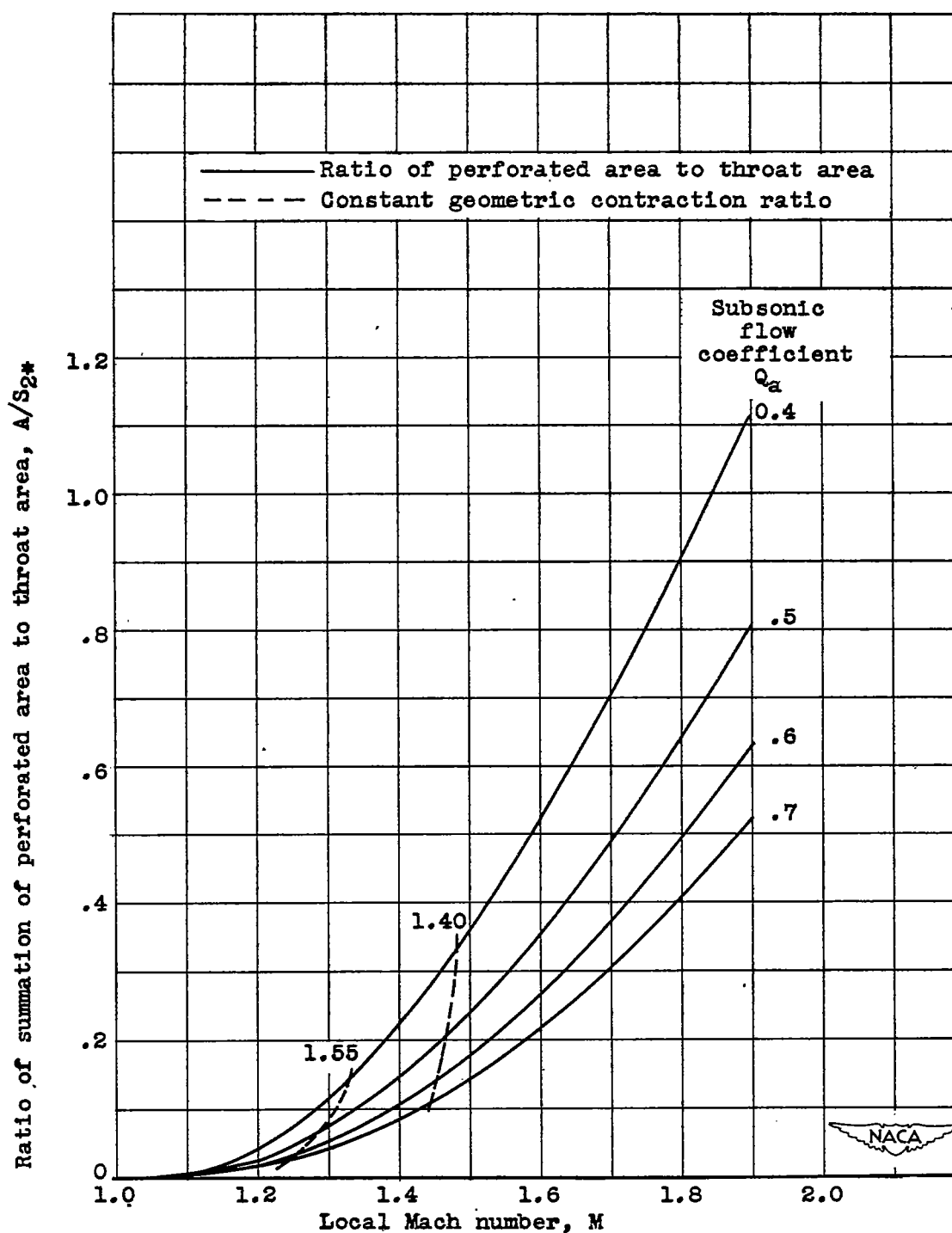


Figure 1. - Theoretical variation of perforated area with local Mach number, Free-stream Mach number M_0 , 1.90.

CONFIDENTIAL

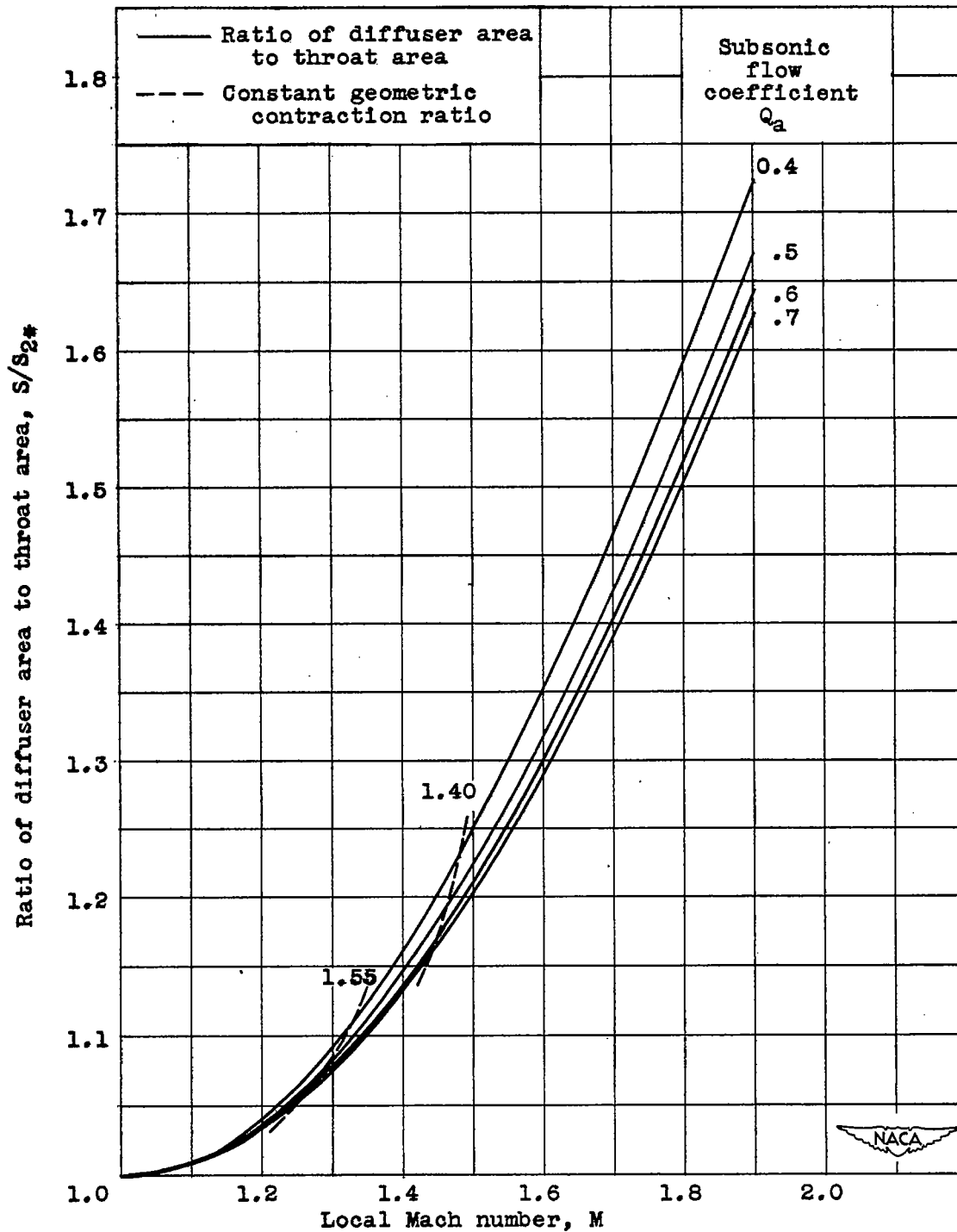


Figure 2. - Theoretical variation of diffuser cross-sectional area with local Mach number. Free-stream Mach number M_0 , 1.90.

CONFIDENTIAL

1254

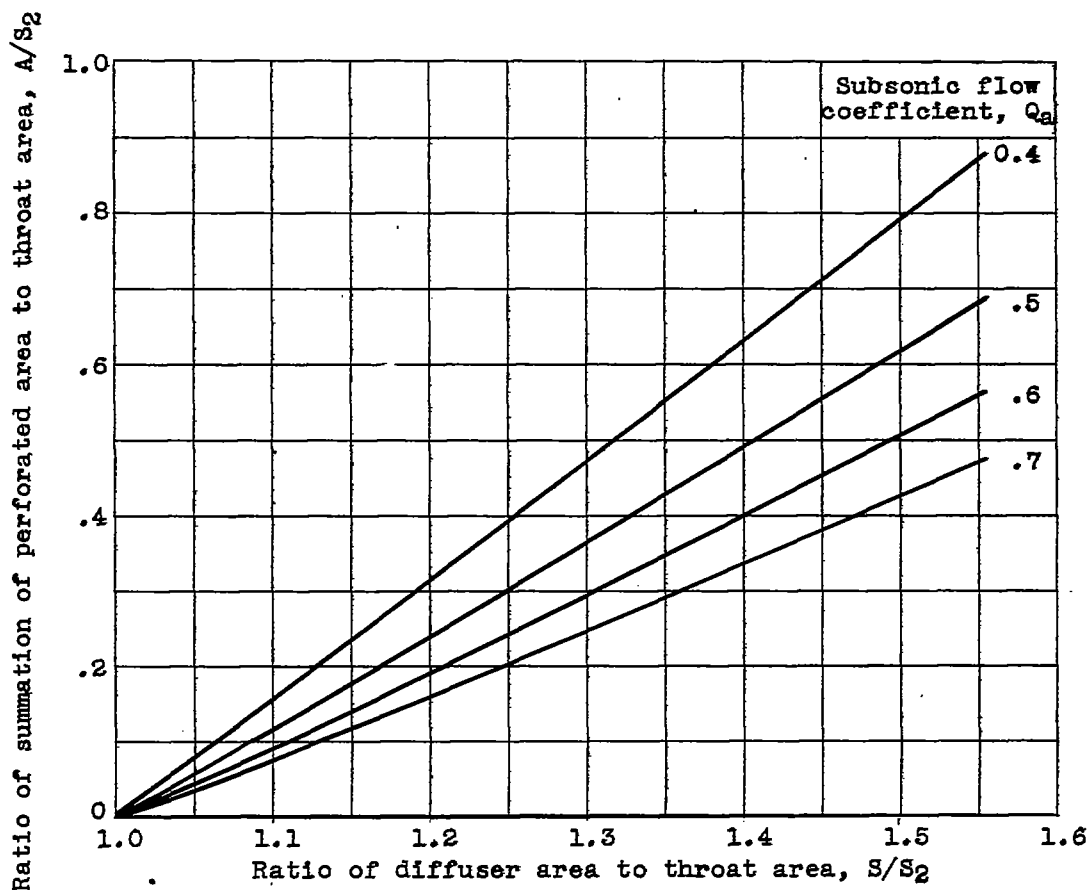


Figure 3. - Theoretical distribution of perforations along diffuser inlet. Contraction ratio, 1.55; free-stream Mach number M_0 , 1.90.

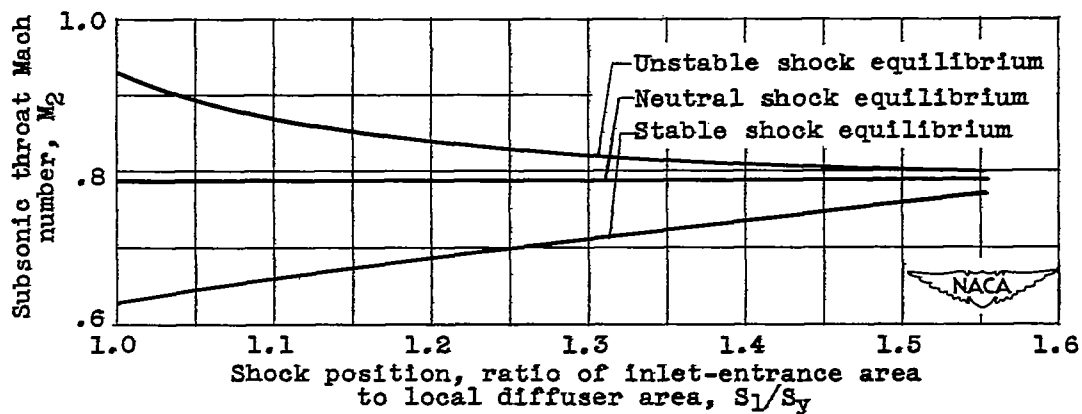


Figure 4. - Variation of subsonic throat Mach number with shock position for three perforation distributions. Contraction ratio, 1.55; subsonic flow coefficient Q_a , 0.5; free-stream Mach number M_0 , 1.90.

CONFIDENTIAL

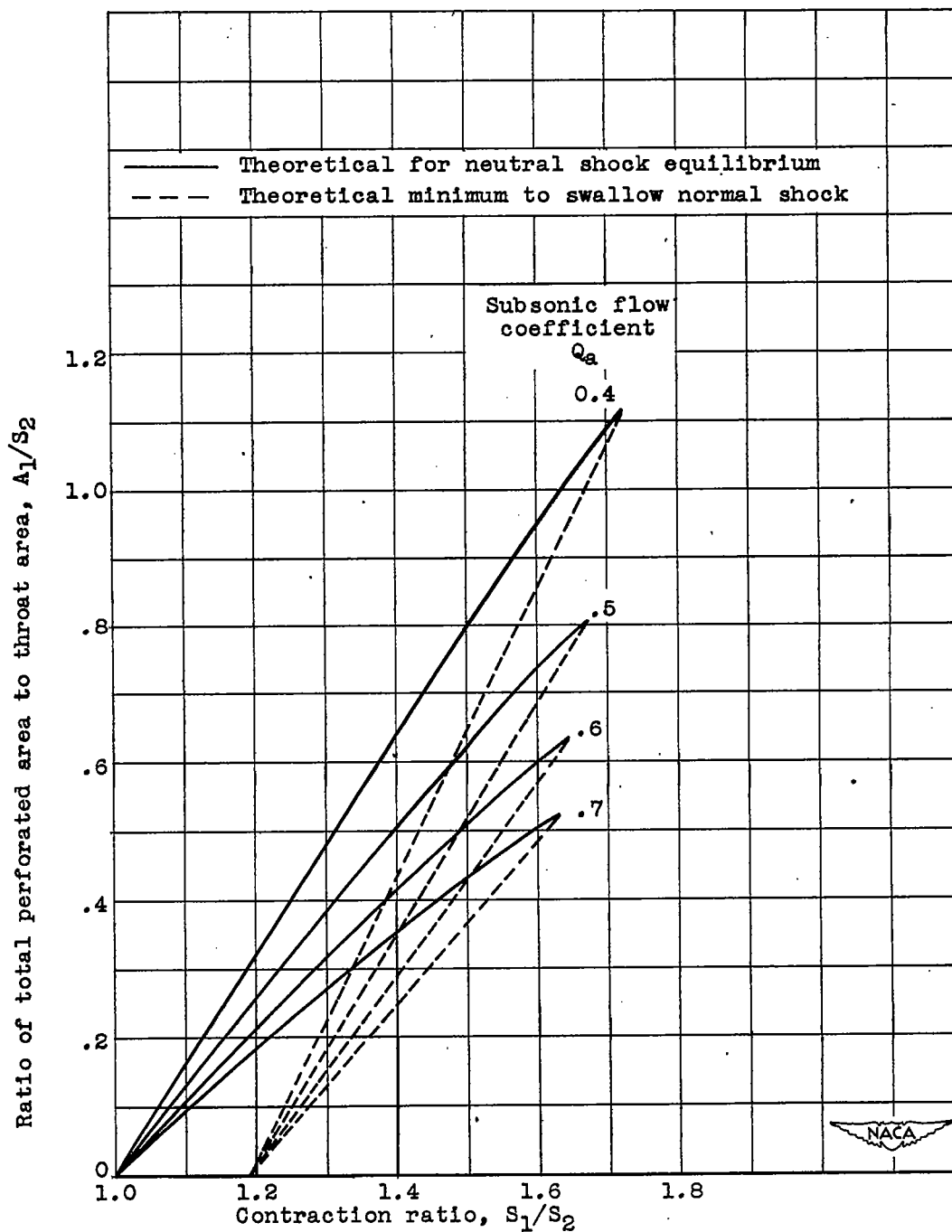
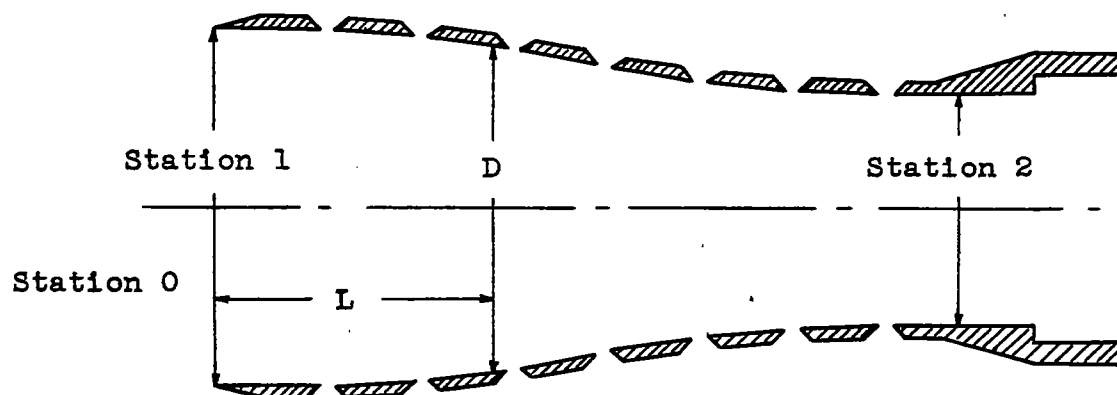


Figure 5. - Comparison of theoretical total-perforated-area to throat-area ratio as function of contraction ratio for swallowing normal shock and for neutral shock equilibrium. Free-stream Mach number M_0 , 1.90.

CONFIDENTIAL

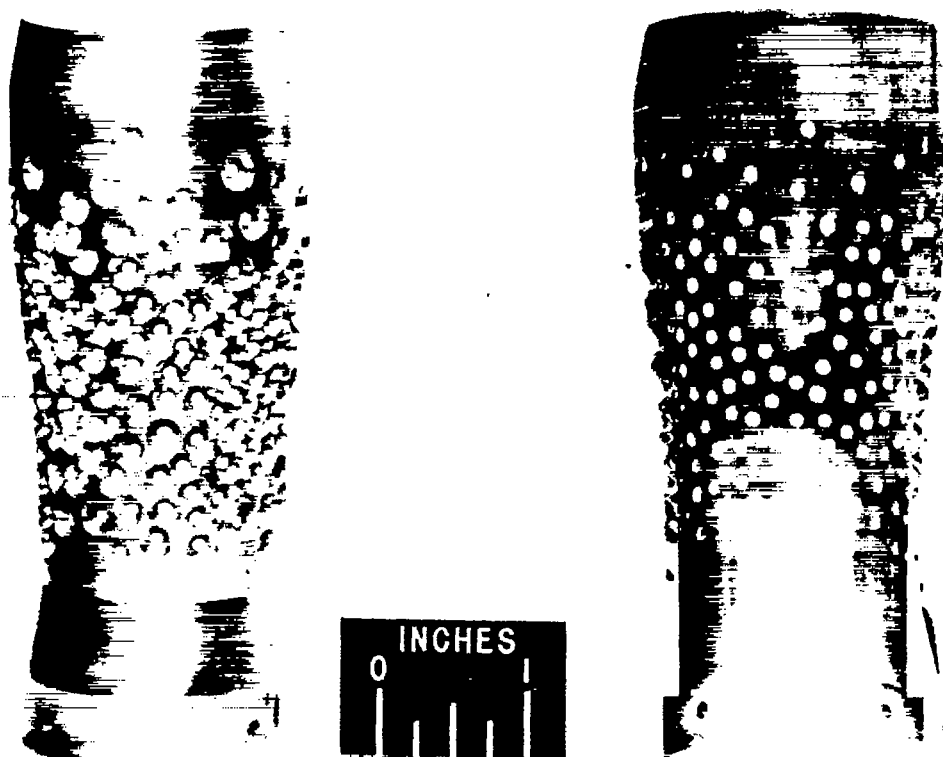


| Length L (in.) | Diameter, D (in.) | | | | | | |
|----------------------|------------------------------|-------|-------|-------|-------|-------|-------|
| | Contraction ratio, S_1/S_2 | | | | | | |
| | 1.402 | 1.490 | 1.531 | 1.553 | 1.589 | 1.630 | 1.703 |
| 0 | 1.826 | 1.882 | 1.908 | 1.921 | 1.944 | 1.969 | 2.012 |
| .25 | | 1.882 | | | | | |
| .50 | | 1.876 | | | | | |
| .75 | 1.826 | 1.862 | 1.908 | 1.921 | 1.944 | 1.969 | 2.012 |
| 1.00 | 1.819 | 1.832 | 1.901 | 1.914 | 1.936 | 1.961 | 2.005 |
| 1.25 | 1.804 | 1.794 | 1.883 | 1.895 | 1.917 | 1.942 | 1.984 |
| 1.50 | 1.780 | 1.752 | 1.855 | 1.869 | 1.888 | 1.911 | 1.951 |
| 1.75 | 1.748 | 1.710 | 1.815 | 1.830 | 1.846 | 1.866 | 1.903 |
| 2.00 | 1.709 | 1.670 | 1.766 | 1.782 | 1.793 | 1.810 | 1.839 |
| 2.25 | 1.668 | 1.628 | 1.712 | 1.725 | 1.733 | 1.747 | 1.767 |
| 2.50 | 1.632 | 1.588 | 1.663 | 1.673 | 1.680 | 1.690 | 1.703 |
| 2.75 | 1.601 | 1.560 | 1.622 | 1.629 | 1.634 | 1.641 | 1.649 |
| 3.00 | 1.576 | 1.546 | 1.589 | 1.593 | 1.597 | 1.600 | 1.605 |
| 3.25 | 1.557 | 1.542 | 1.563 | 1.566 | 1.567 | 1.570 | 1.572 |
| 3.50 | 1.546 | | 1.548 | 1.548 | 1.549 | 1.550 | 1.550 |
| 3.75 | 1.542 | | 1.542 | 1.542 | 1.542 | 1.542 | 1.542 |
| 4.25 | | 1.542 | | | | | |
| 4.75 | 1.542 | | 1.542 | 1.542 | 1.542 | 1.542 | 1.542 |



Figure 6. - Sketch of typical inlet with table of coordinates for contraction ratios investigated.

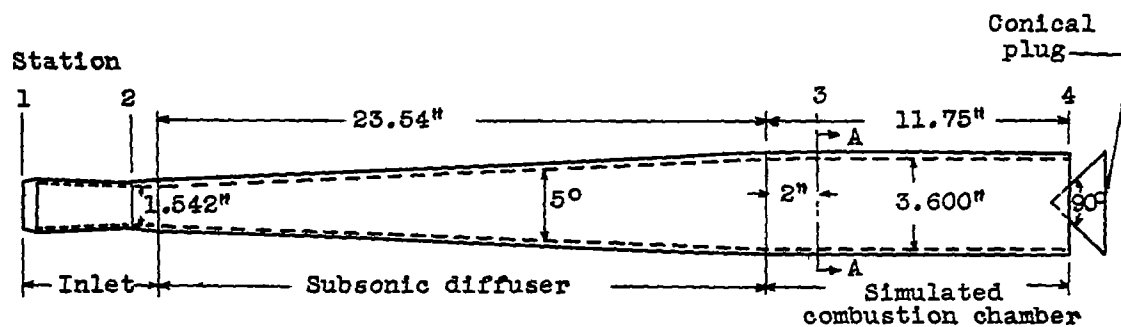




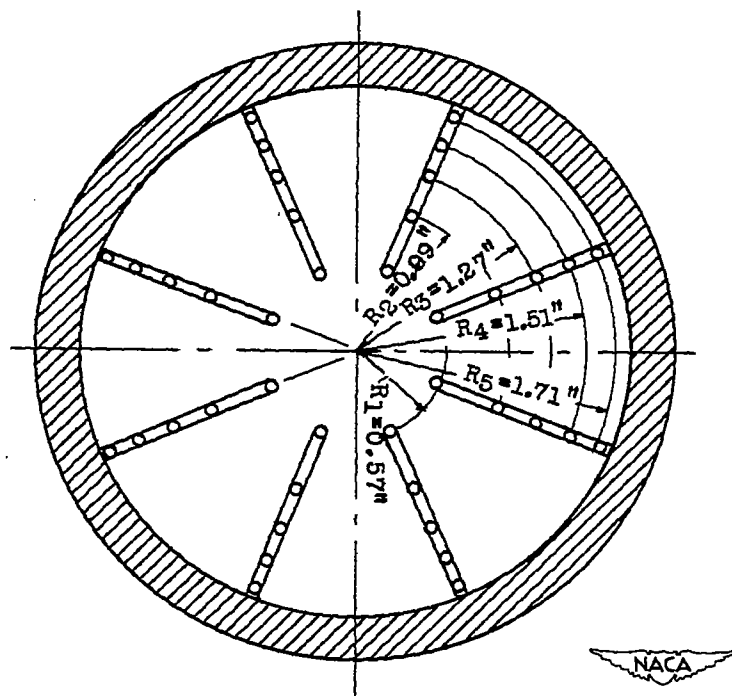
C-21308
4-27-48

Figure 7. - Photograph of inlet 1.59-e illustrating distribution of perforations.

1254



(a) Schematic diagram showing component parts.



(b) Pitot-static survey rake located at station A-A.

Figure 8. - Sketch of experimental model.

CONFIDENTIAL

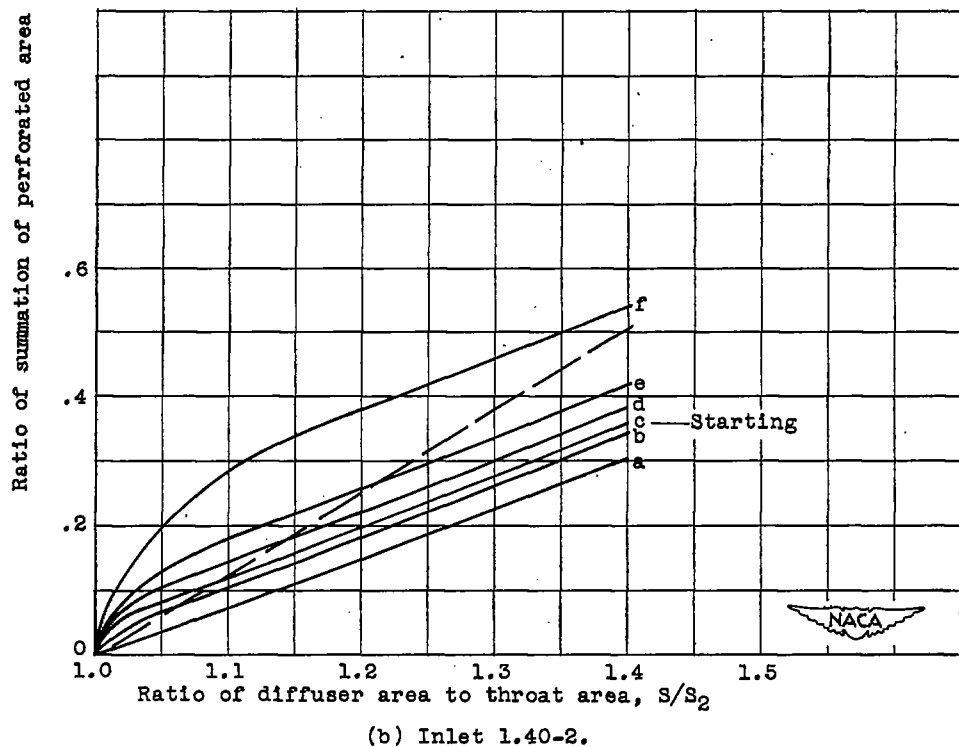
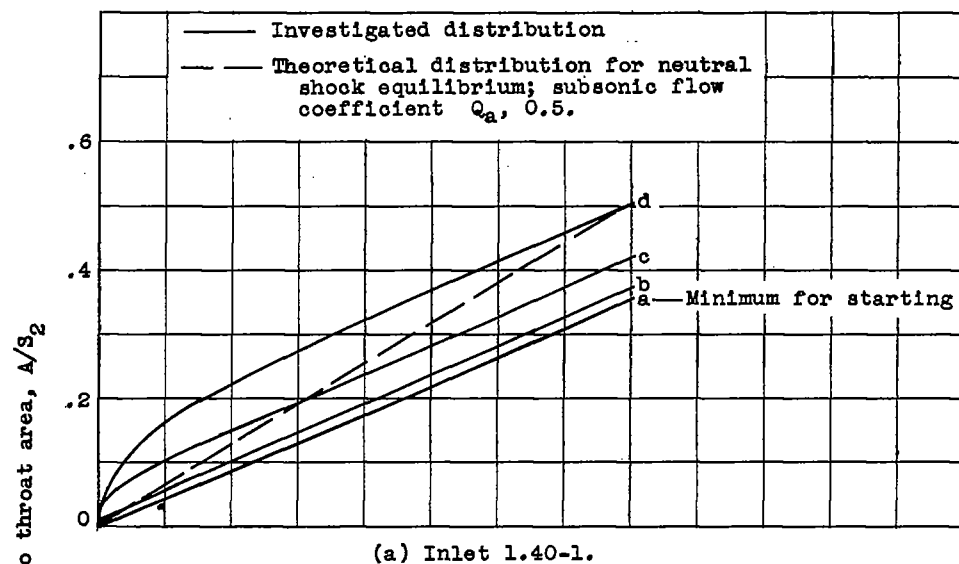


Figure 9. - Distribution of perforations along diffuser inlet.

CONFIDENTIAL

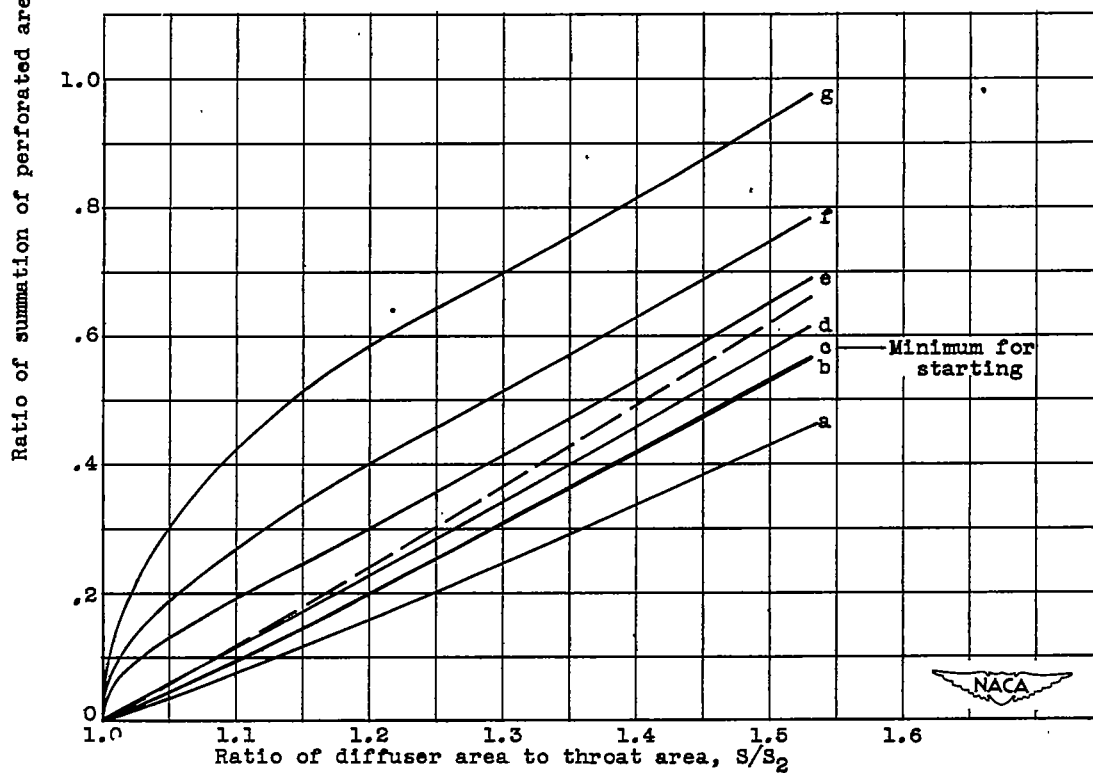
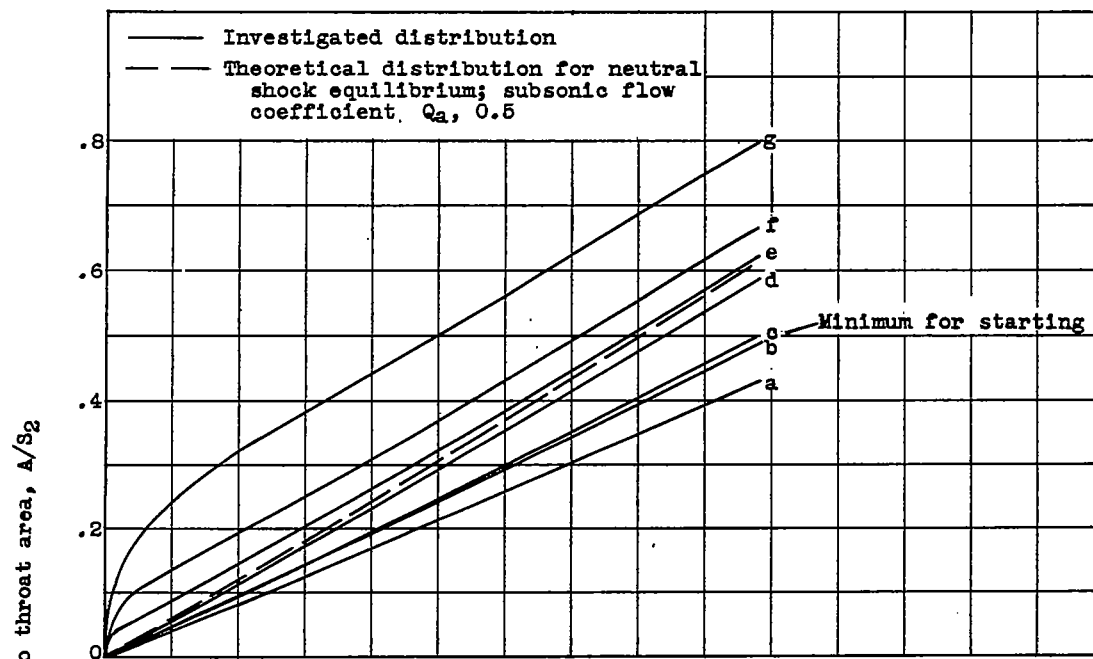
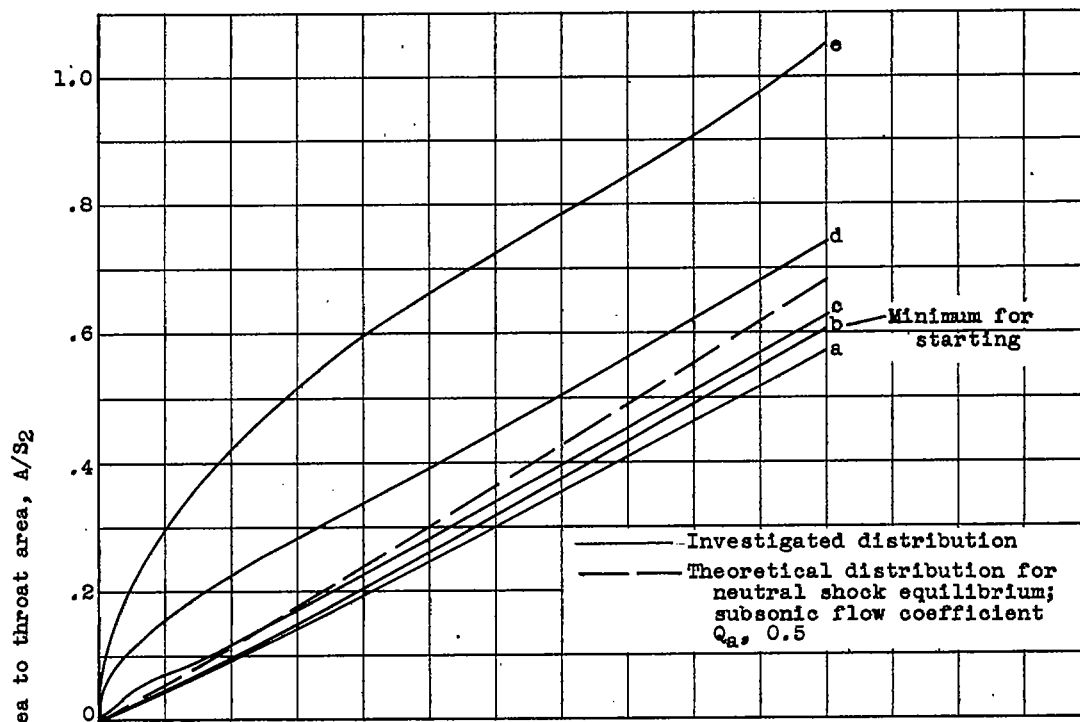
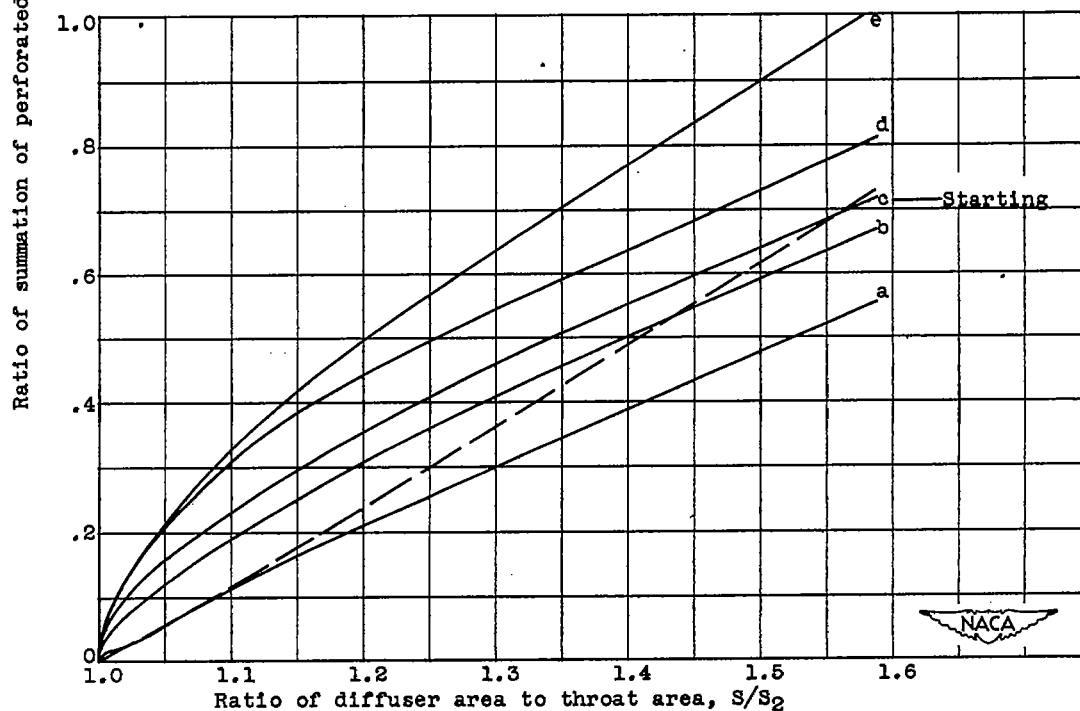


Figure 9. - Continued. Distribution of perforations along diffuser inlet.



(e) Inlet 1.55.



(f) Inlet 1.59.

Figure 9. - Continued. Distribution of perforations along diffuser inlet.

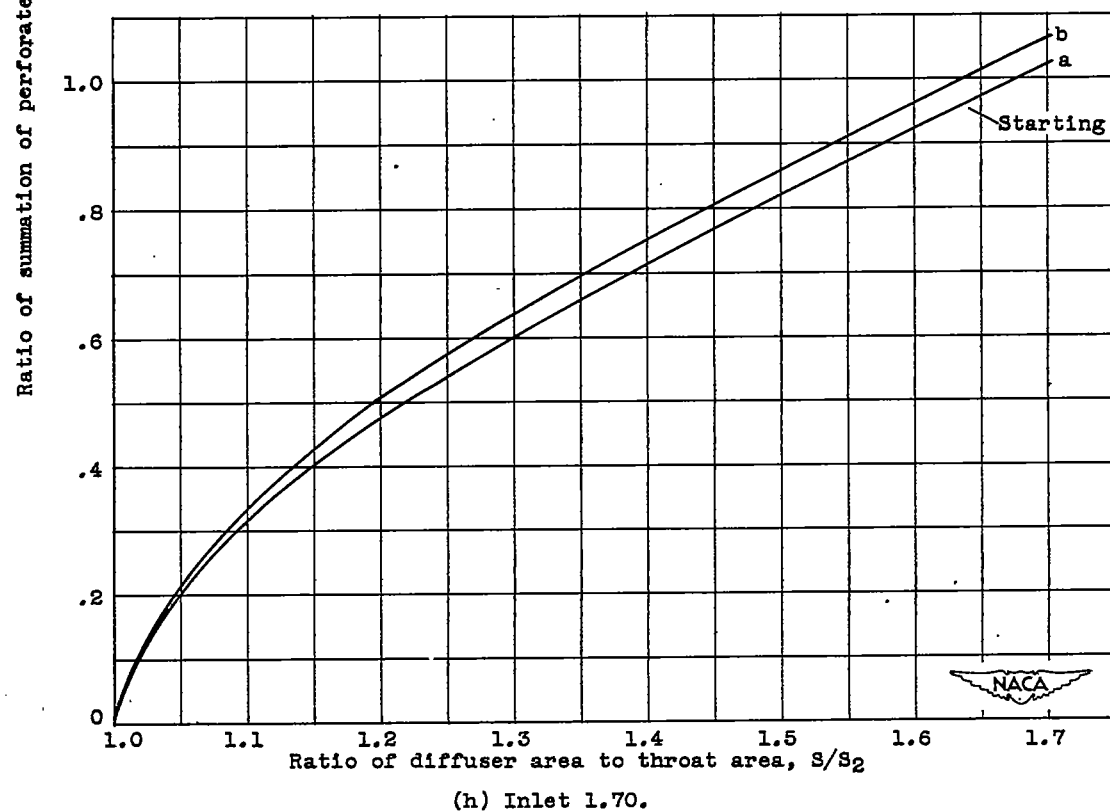
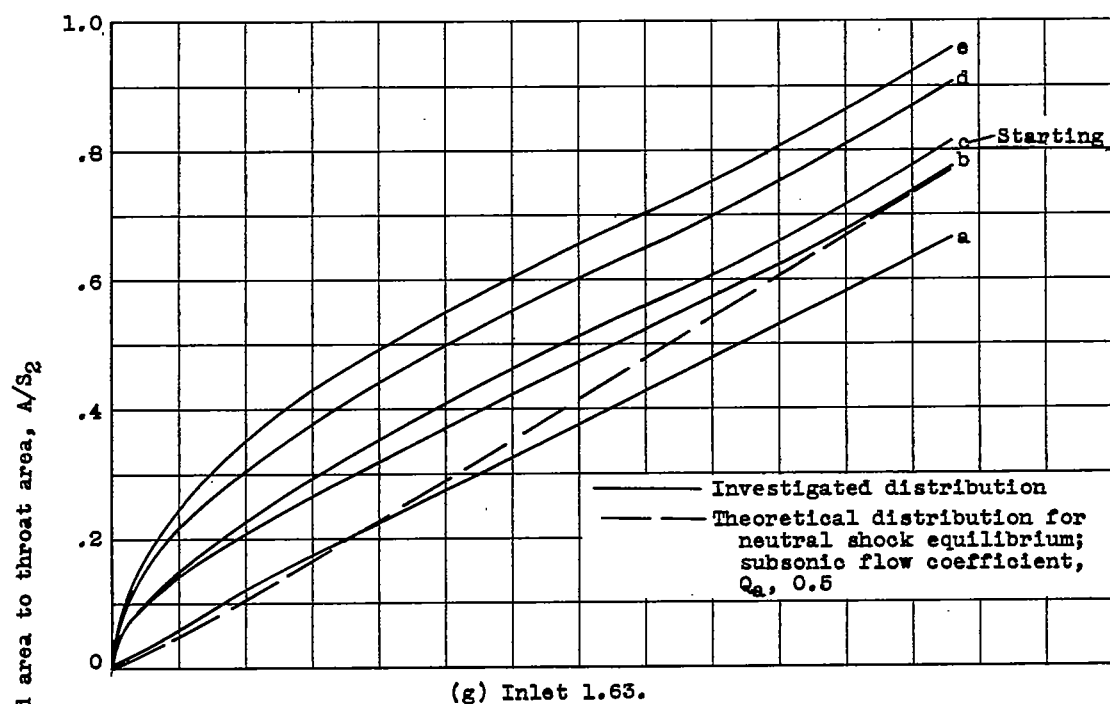


Figure 9. - Concluded. Distribution of perforations along diffuser inlet.

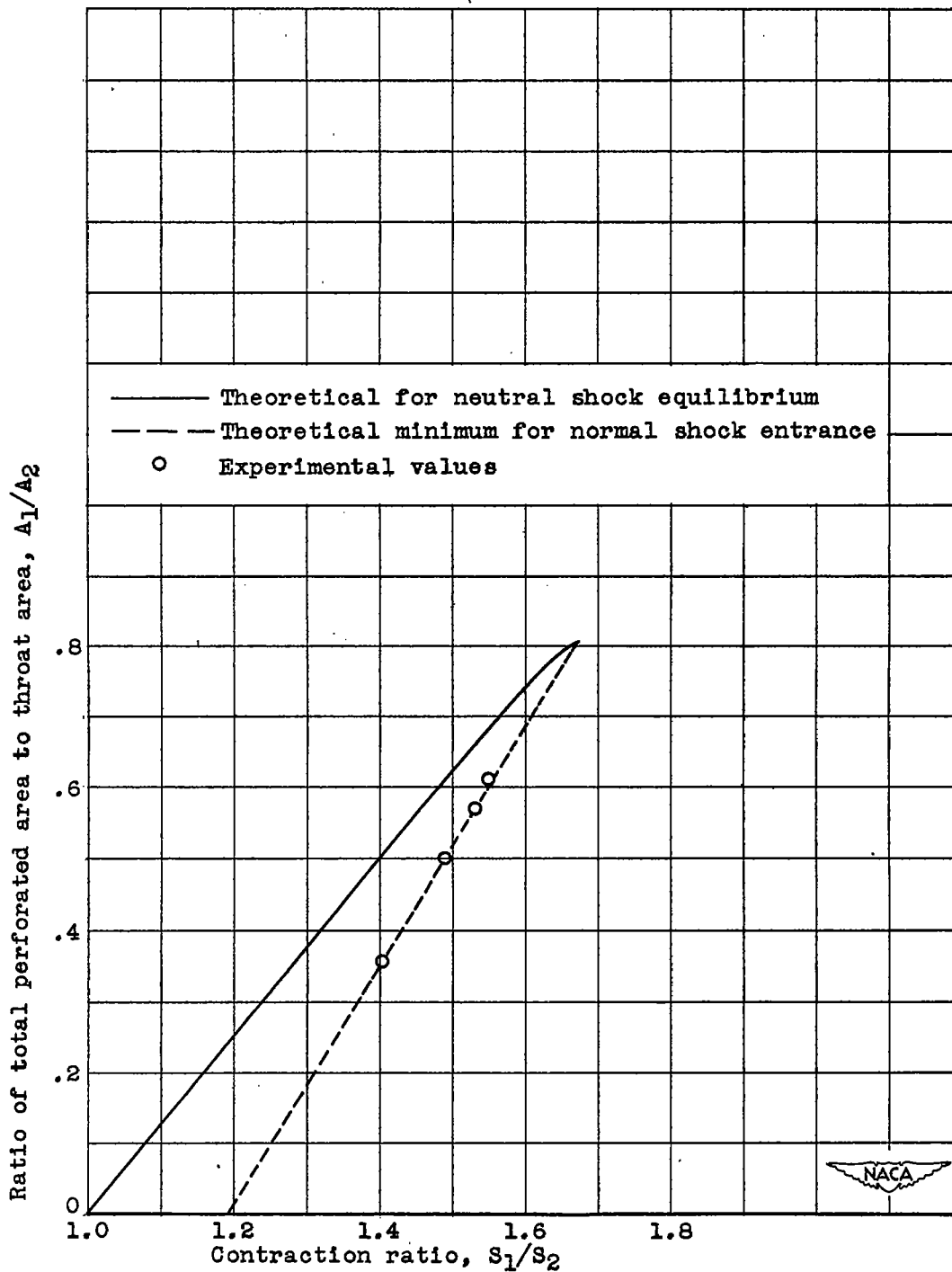


Figure 10. - Ratio of total perforated area to throat area as function of contraction ratio for starting and neutral shock equilibrium. Subsonic flow coefficient Q_a , 0.5; free-stream Mach number M_0 , 1.90.

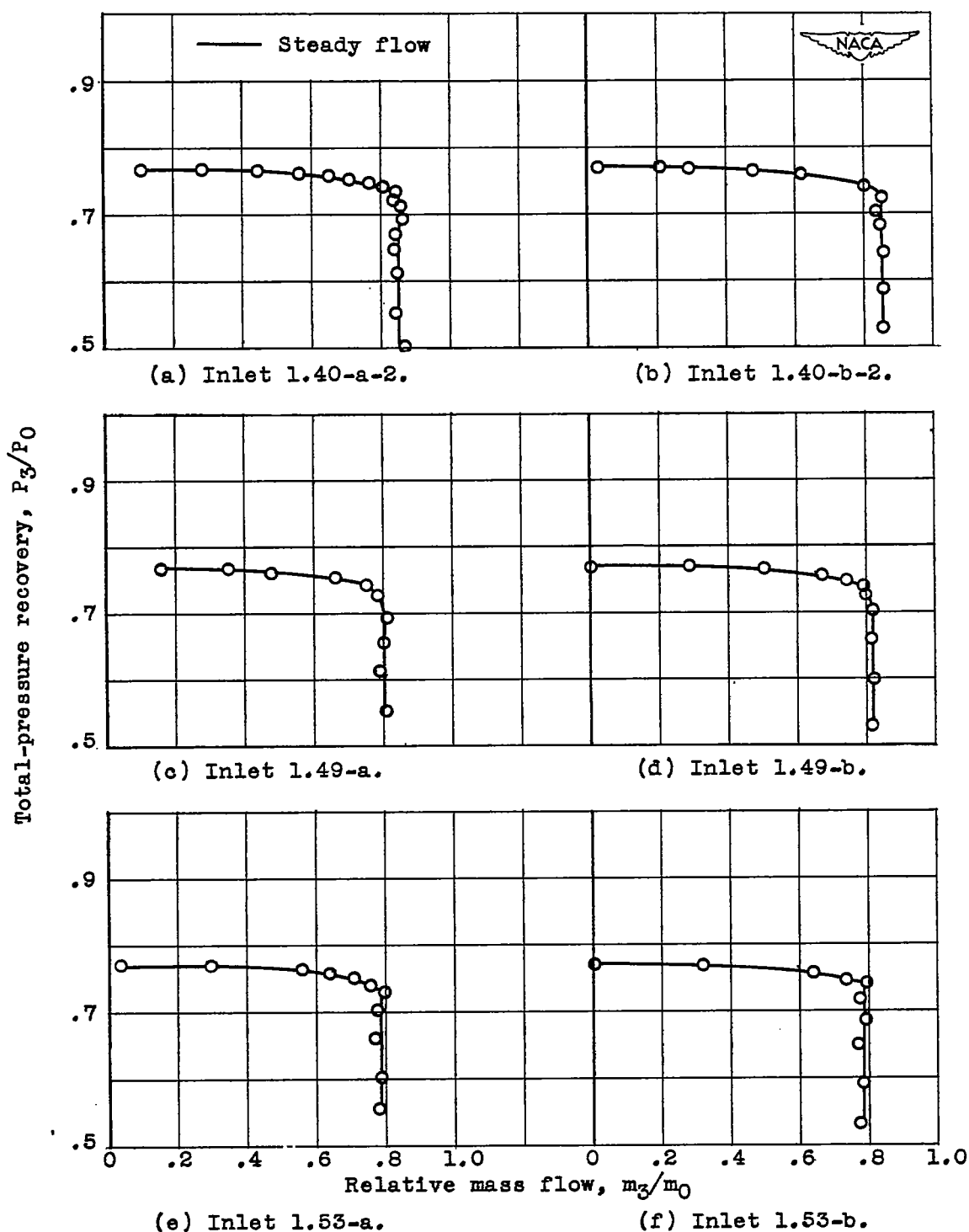


Figure 11. - Variation of total-pressure recovery with relative mass flow for inlets having insufficient perforations to permit normal shock entrance. Free-stream Mach number M_0 , 1.90.

CONFIDENTIAL

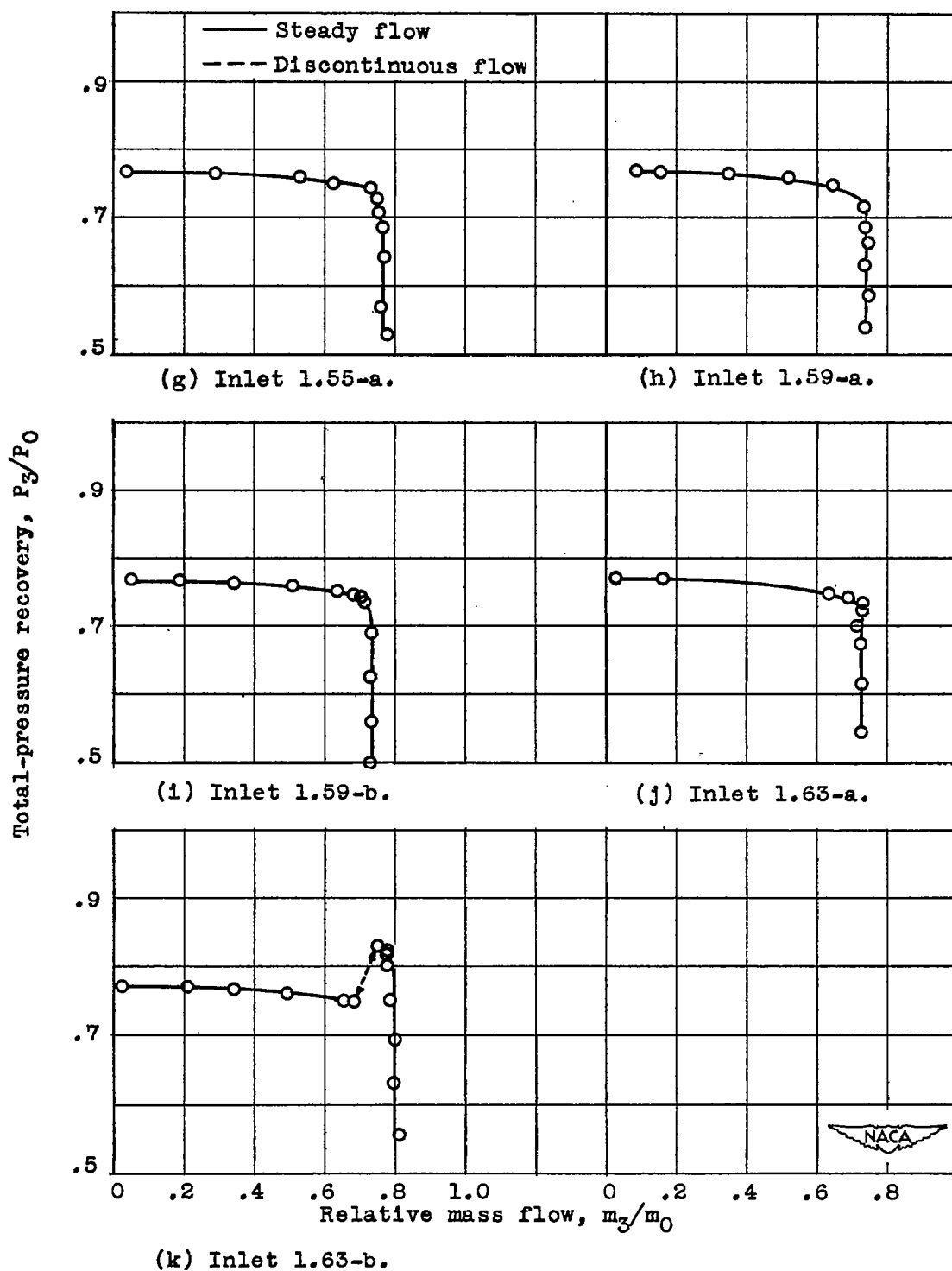


Figure 11. - Concluded. Variation of total-pressure recovery with relative mass flow for inlets having insufficient perforations to permit normal shock entrance. Free-stream Mach number M_0 , 1.90.

CONFIDENTIAL

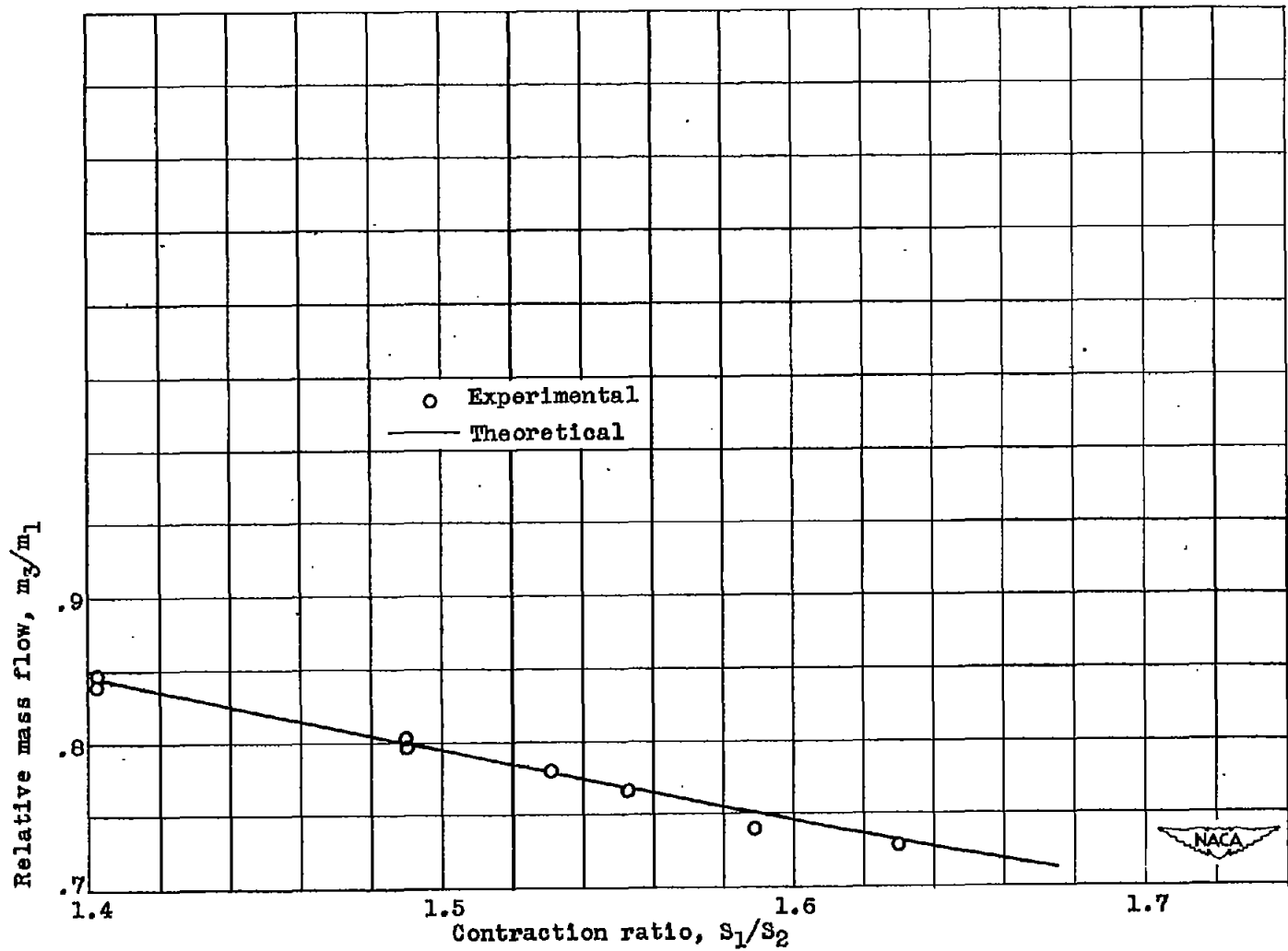


Figure 12. - Relative mass flow (supercritical) as function of contraction ratio for inlets having insufficient perforations to permit normal shock entrance.

CONFIDENTIAL

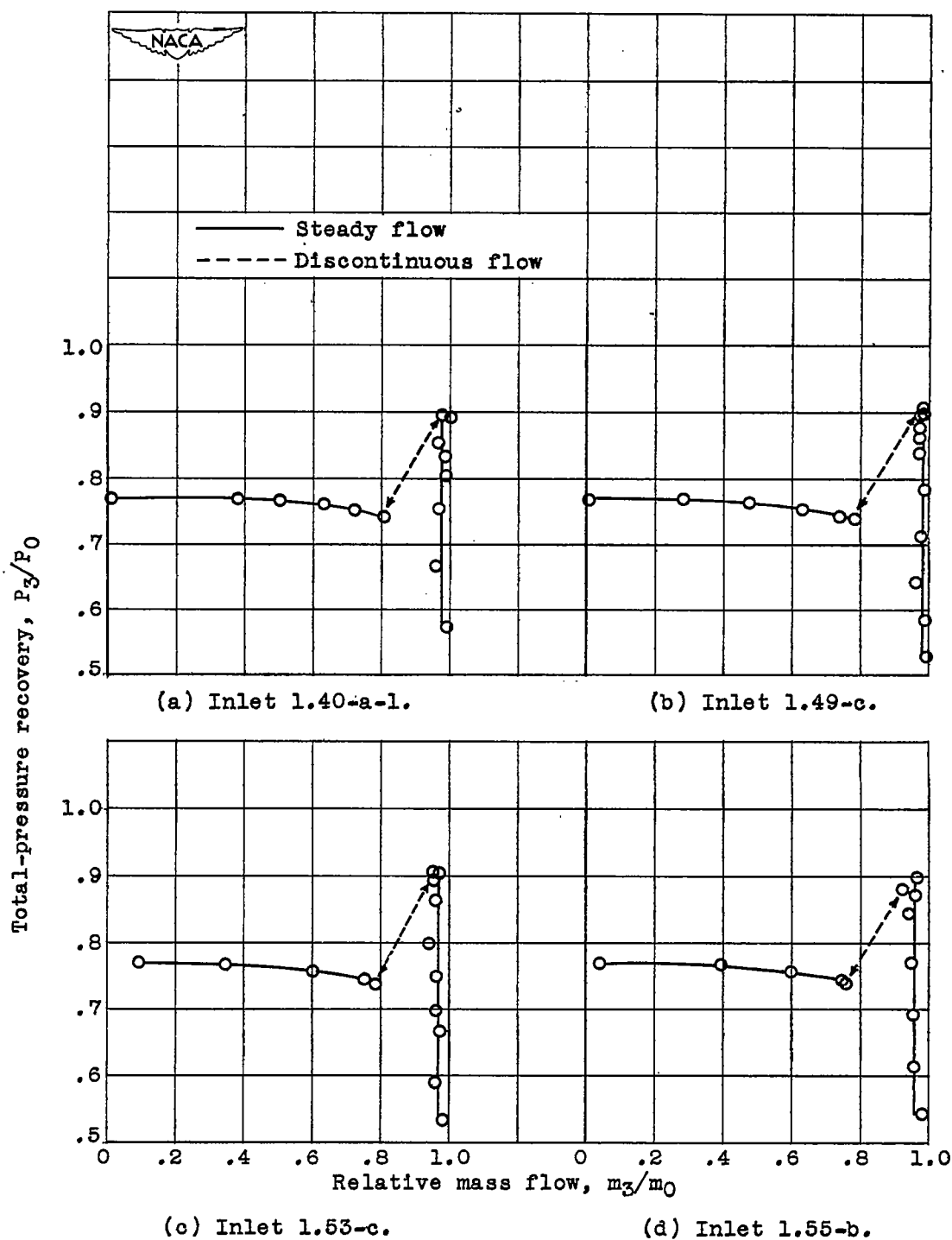


Figure 13. - Variation of total-pressure recovery with relative mass flow for inlets having just sufficient perforations to permit normal shock entrance. Free-stream Mach number M_0 , 1.90.

CONFIDENTIAL

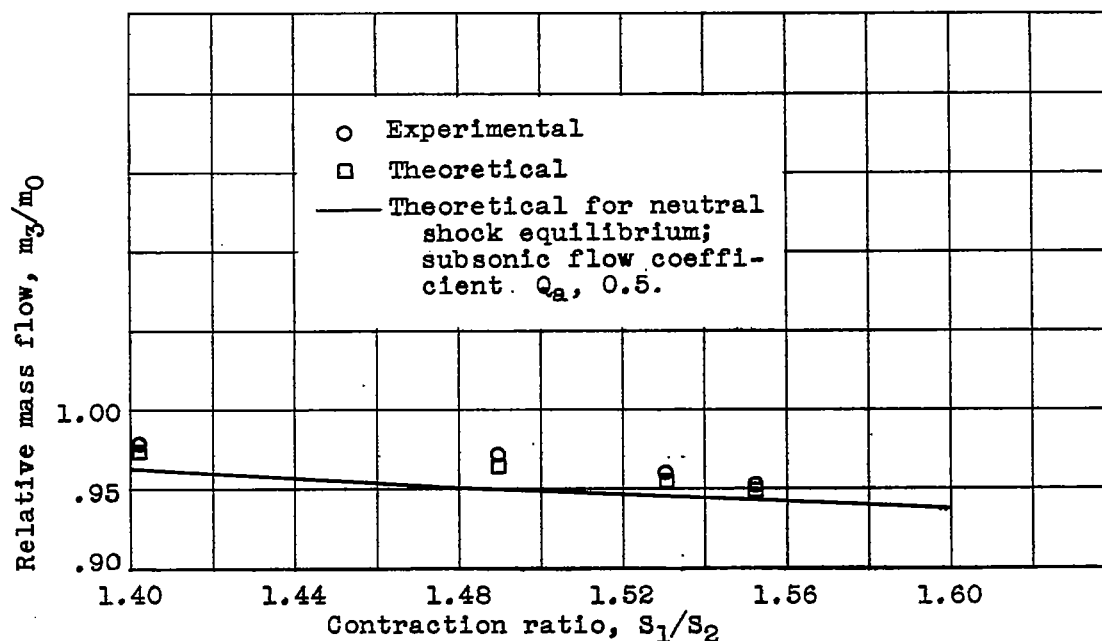


Figure 14. - Relative mass flow (supercritical) as function of contraction ratio for inlets having just sufficient perforations to permit normal shock entrance. Free-stream Mach number M_0 , 1.90.

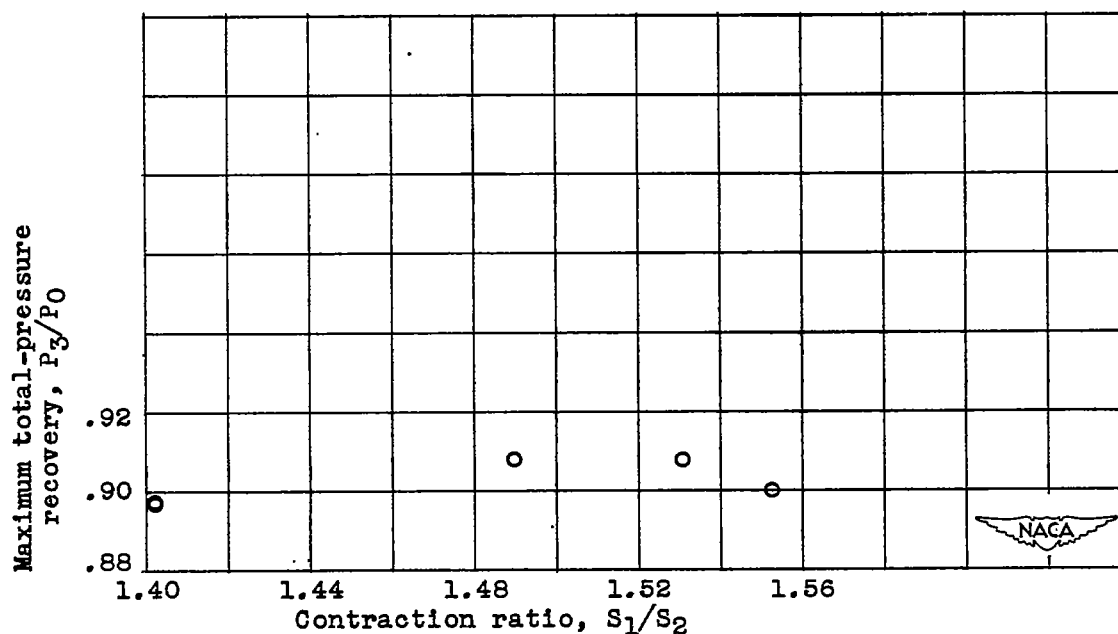


Figure 15. - Variation of maximum total-pressure recovery with contraction ratio for inlets having just sufficient perforations to permit normal shock entrance. Free-stream Mach number M_0 , 1.90.

CONFIDENTIAL

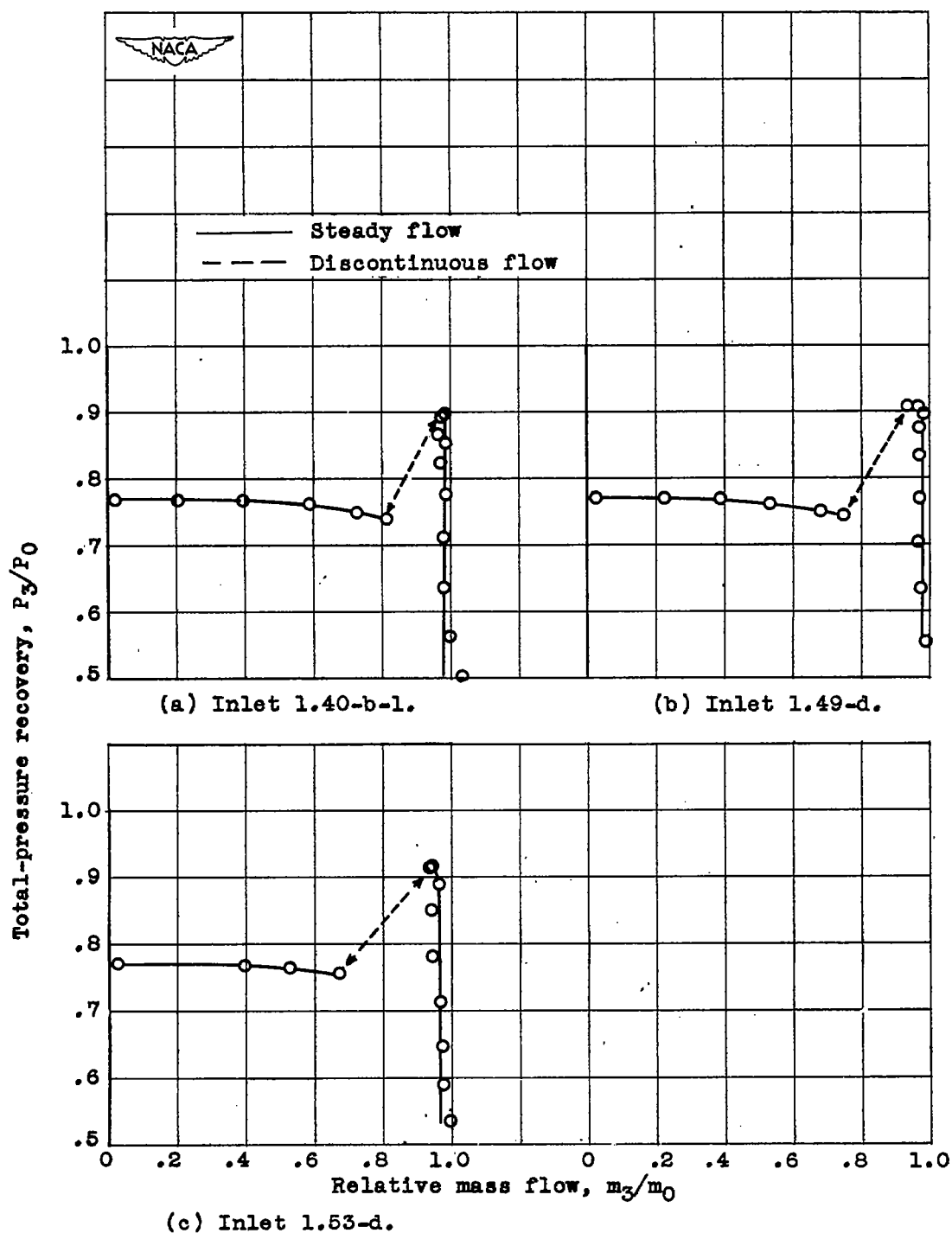
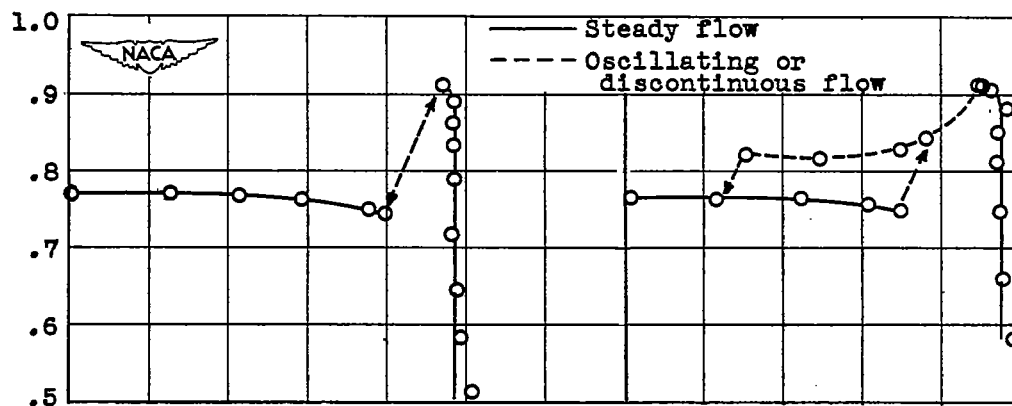


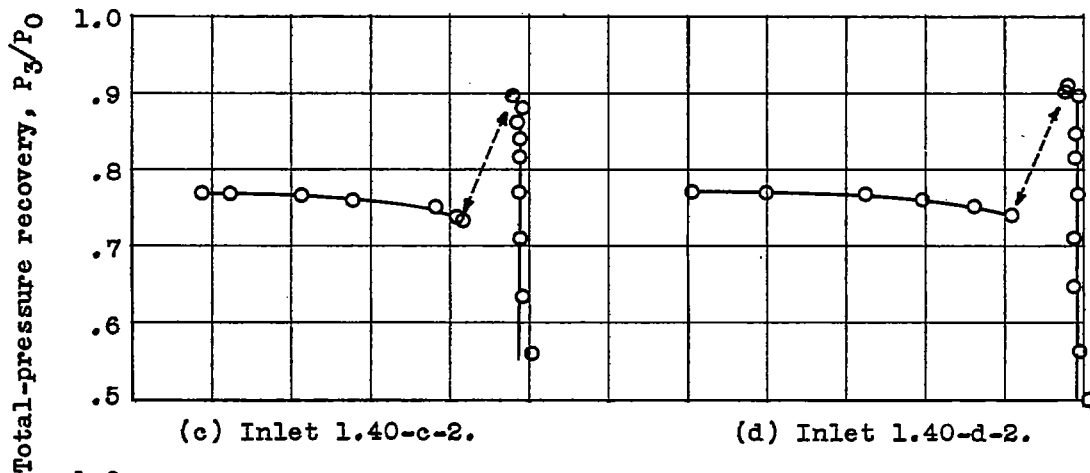
Figure 16. - Variation of total-pressure recovery with relative mass flow for inlets having more than sufficient perforations to permit normal shock entrance and less than those required for neutral shock equilibrium. Free-stream Mach number M_0 , 1.90.

CONFIDENTIAL



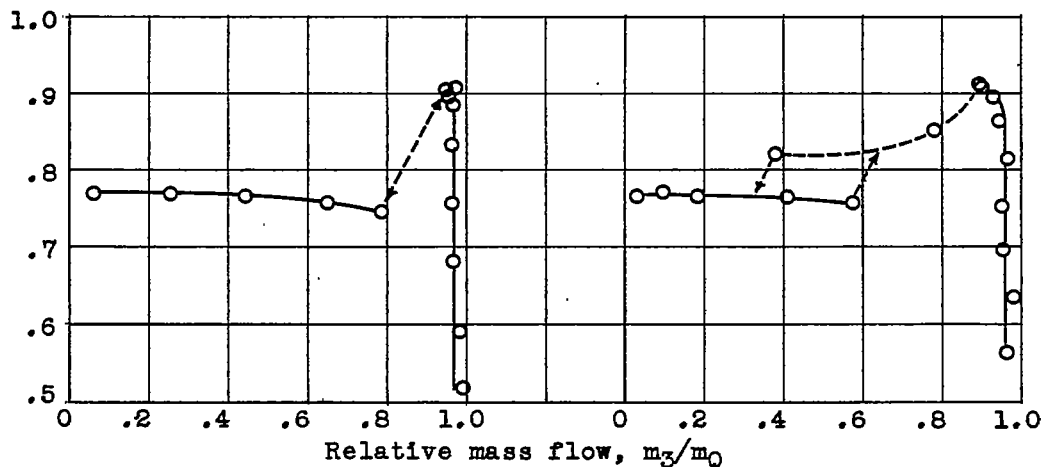
(a) Inlet 1.40-c-1.

(b) Inlet 1.40-d-1.



(c) Inlet 1.40-c-2.

(d) Inlet 1.40-d-2.



(e) Inlet 1.40-e-2.

(f) Inlet 1.40-f-2.

Figure 17. - Variation of total-pressure recovery with relative mass flow for inlets having some region of stable shock equilibrium. Free-stream Mach number M_0 , 1.90.

CONFIDENTIAL

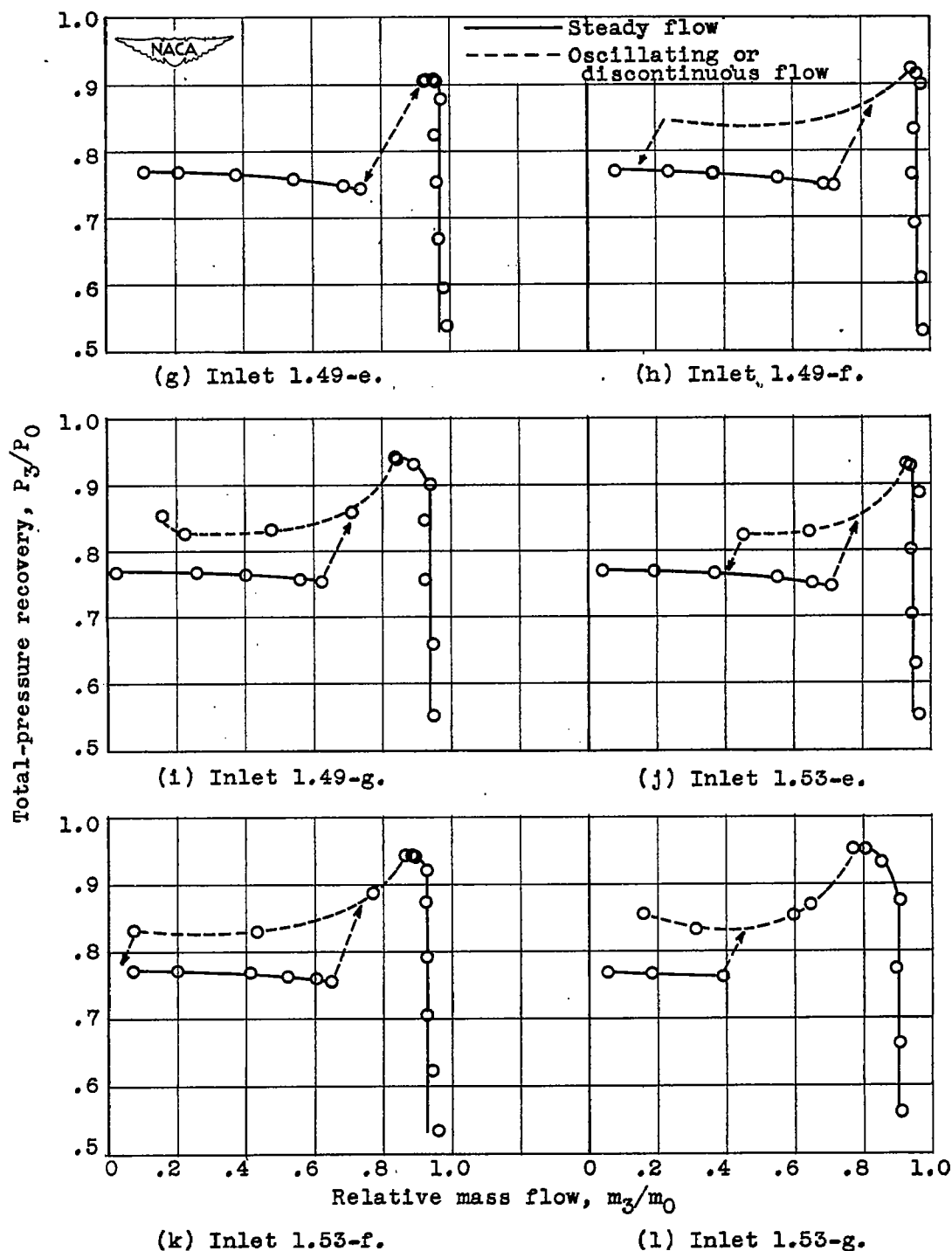


Figure 17. - Continued. Variation of total-pressure recovery with relative mass flow for inlets having some region of stable shock equilibrium. Free-stream Mach number M_0 , 1.90.

CONFIDENTIAL

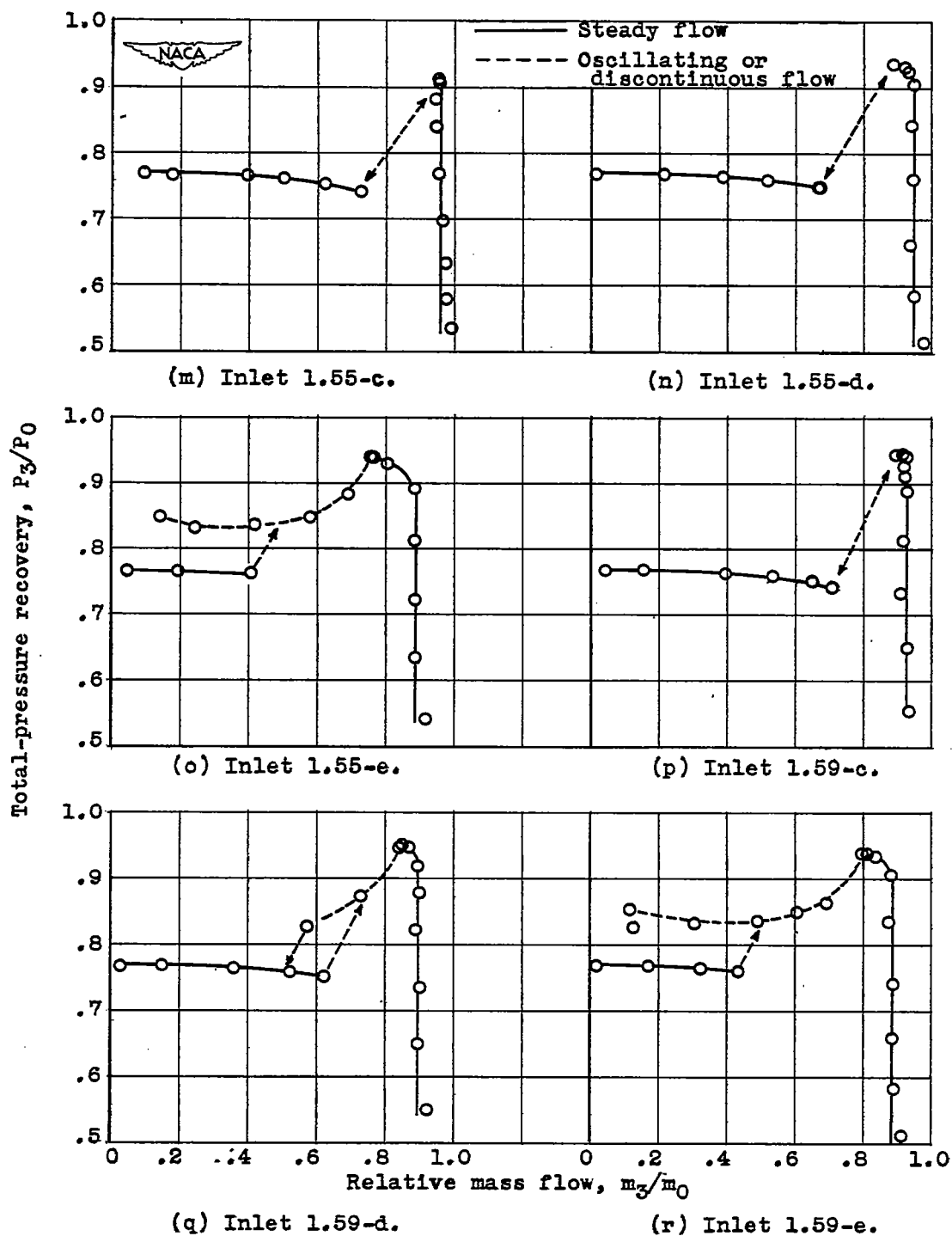


Figure 17. - Continued. Variation of total-pressure recovery with relative mass flow for inlets having some region of stable shock equilibrium. Free-stream Mach number M_0 , 1.90.

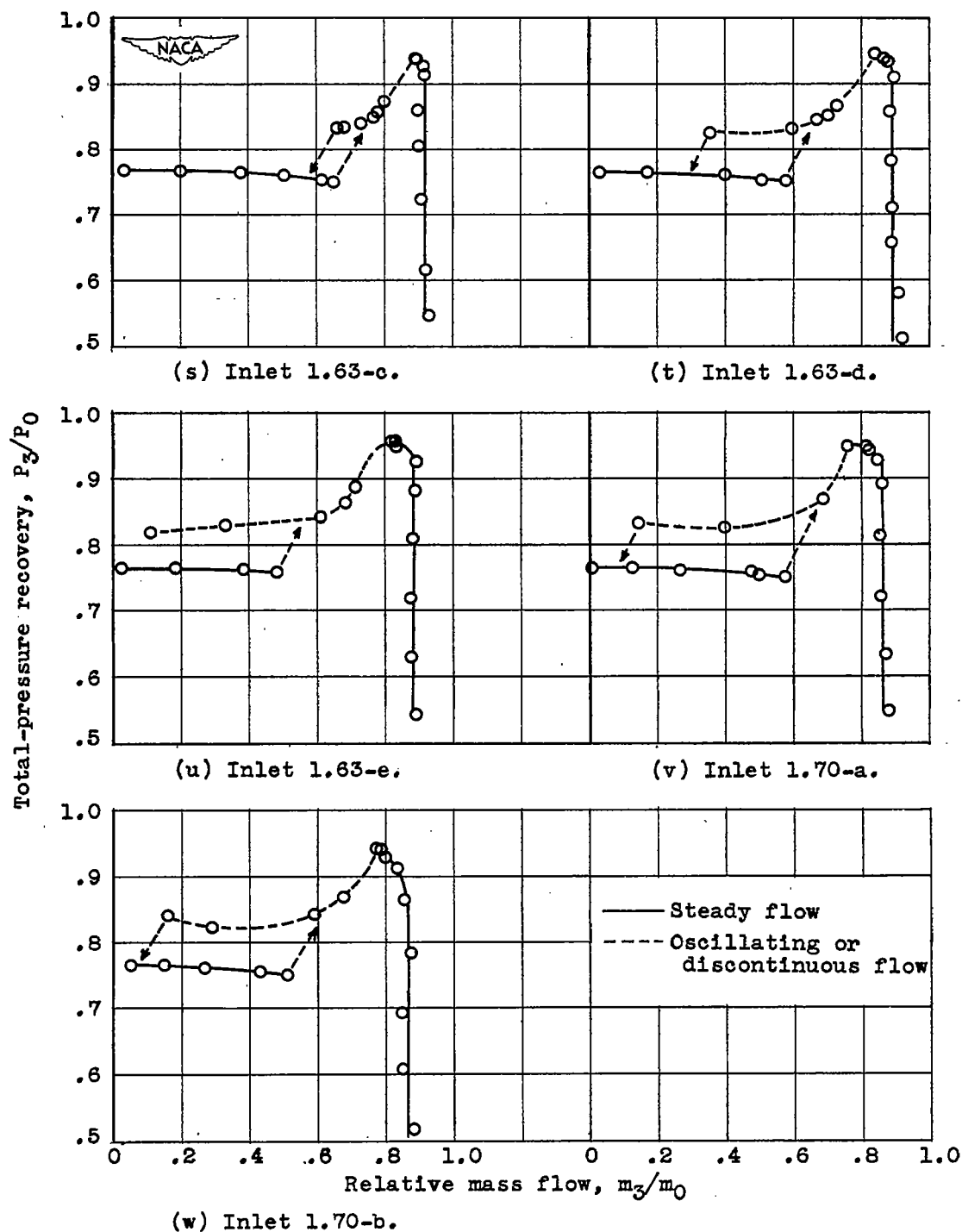


Figure 17. - Concluded. Variation of total-pressure recovery with relative mass flow for inlets having some region of stable shock equilibrium. Free-stream Mach number M_0 , 1.90.

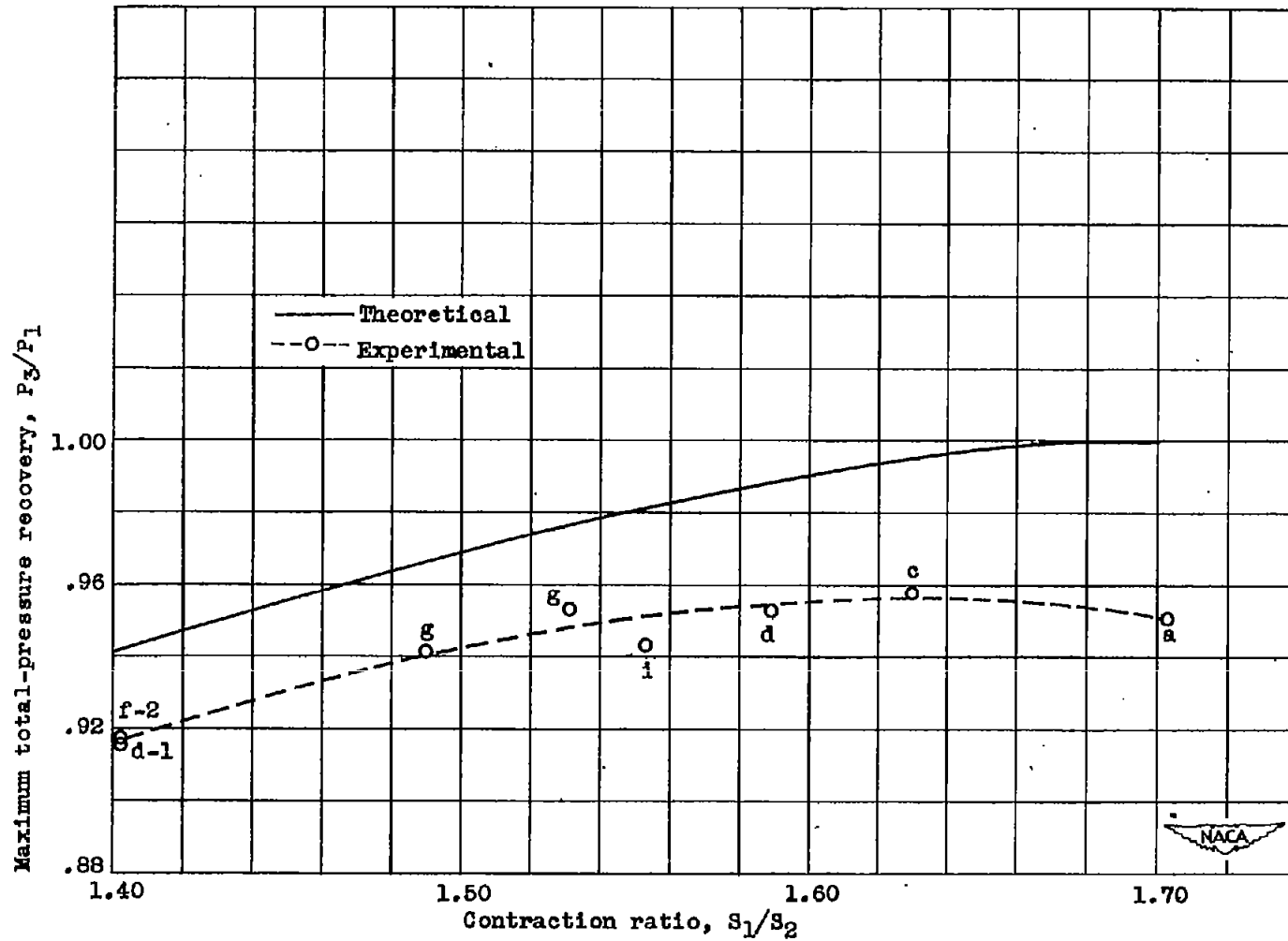
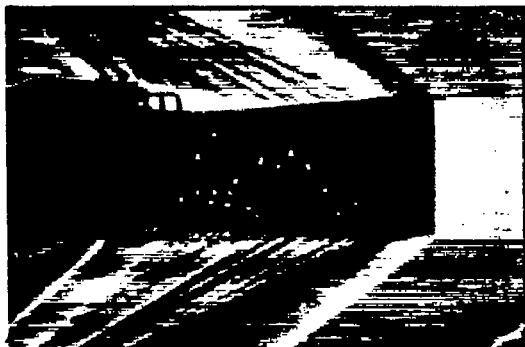


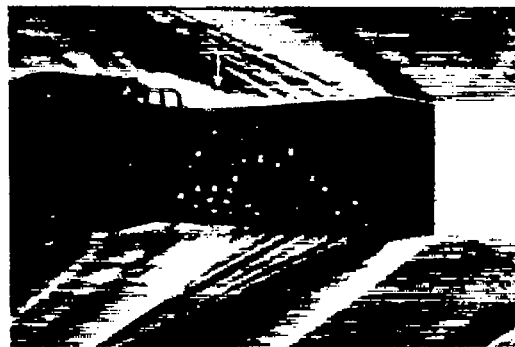
Figure 18. - Variation of maximum total-pressure recovery with contraction ratio. Free-stream Mach number M_0 , 1.90.

1000

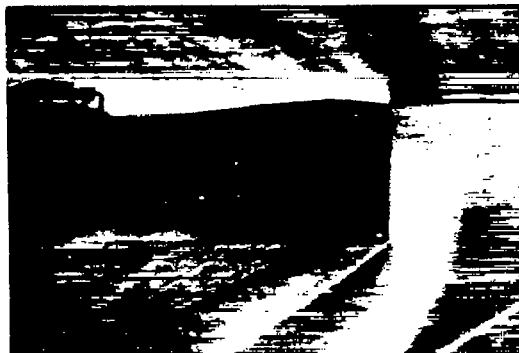
1000



(a) Inlet 1.53-g; P_3/P_0 ,
0.433; m_3/m_1 , 0.91;
exposure, 1/100 second.



(b) Inlet 1.53-g; P_3/P_0 ,
0.953; m_3/m_1 , 0.80;
exposure, 1/100 second.



(c) Inlet 1.70-b; P_3/P_0 ,
0.840; m_3/m_1 , 0.16;
exposure, 1/100 second.

NACA
C-25116
1-31-50



(d) Inlet 1.70-b; P_3/P_0 ,
0.840; m_3/m_1 , 0.16;
exposure, 4 microseconds.



(e) Inlet 1.70-b; P_3/P_0 ,
0.840; m_3/m_1 , 0.16;
exposure, 4 microseconds.

Figure 19. - Schlieren photographs of typical flow patterns about several perforated inlets. Free-stream Mach number M_0 , 1.90.

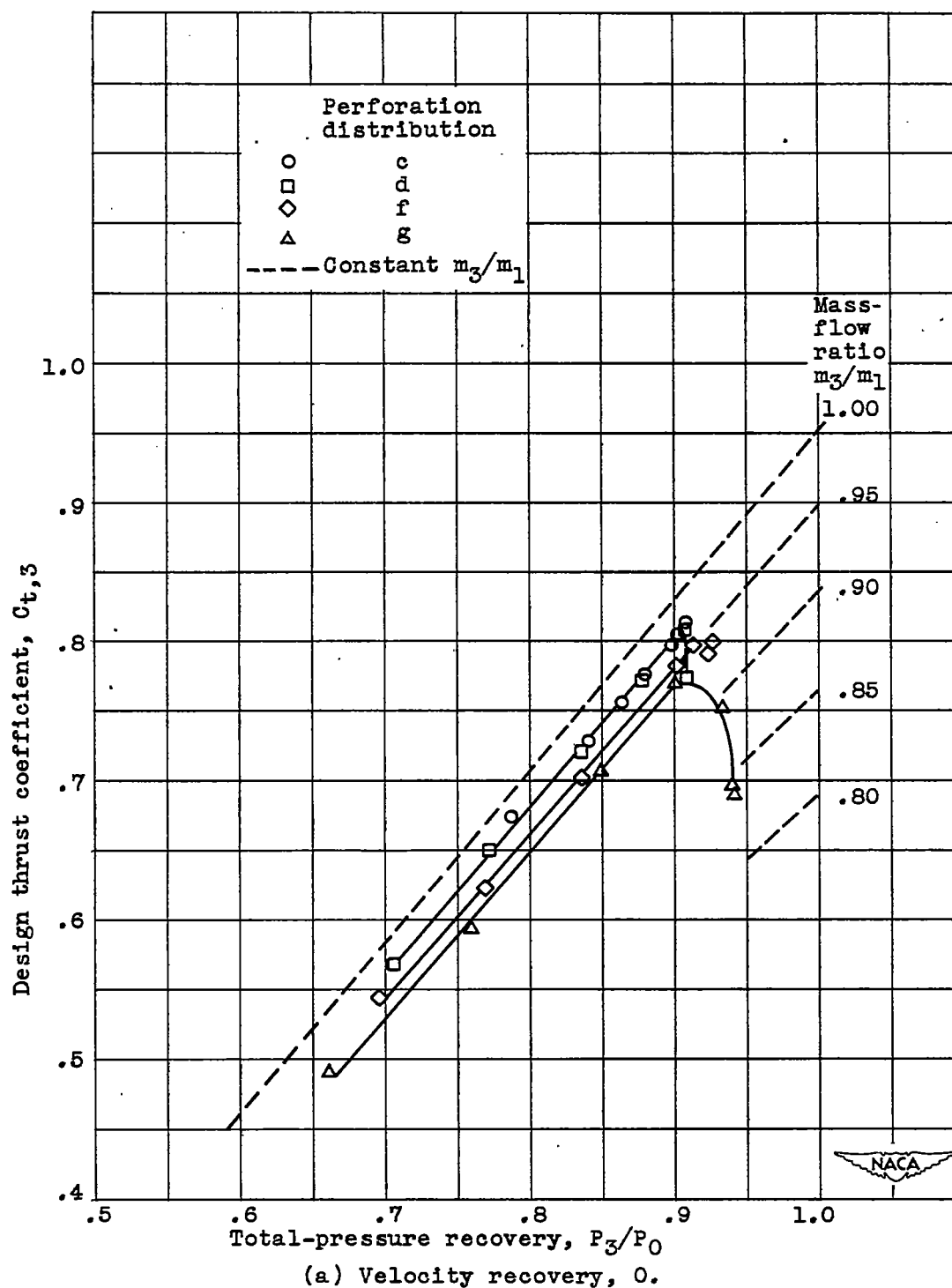
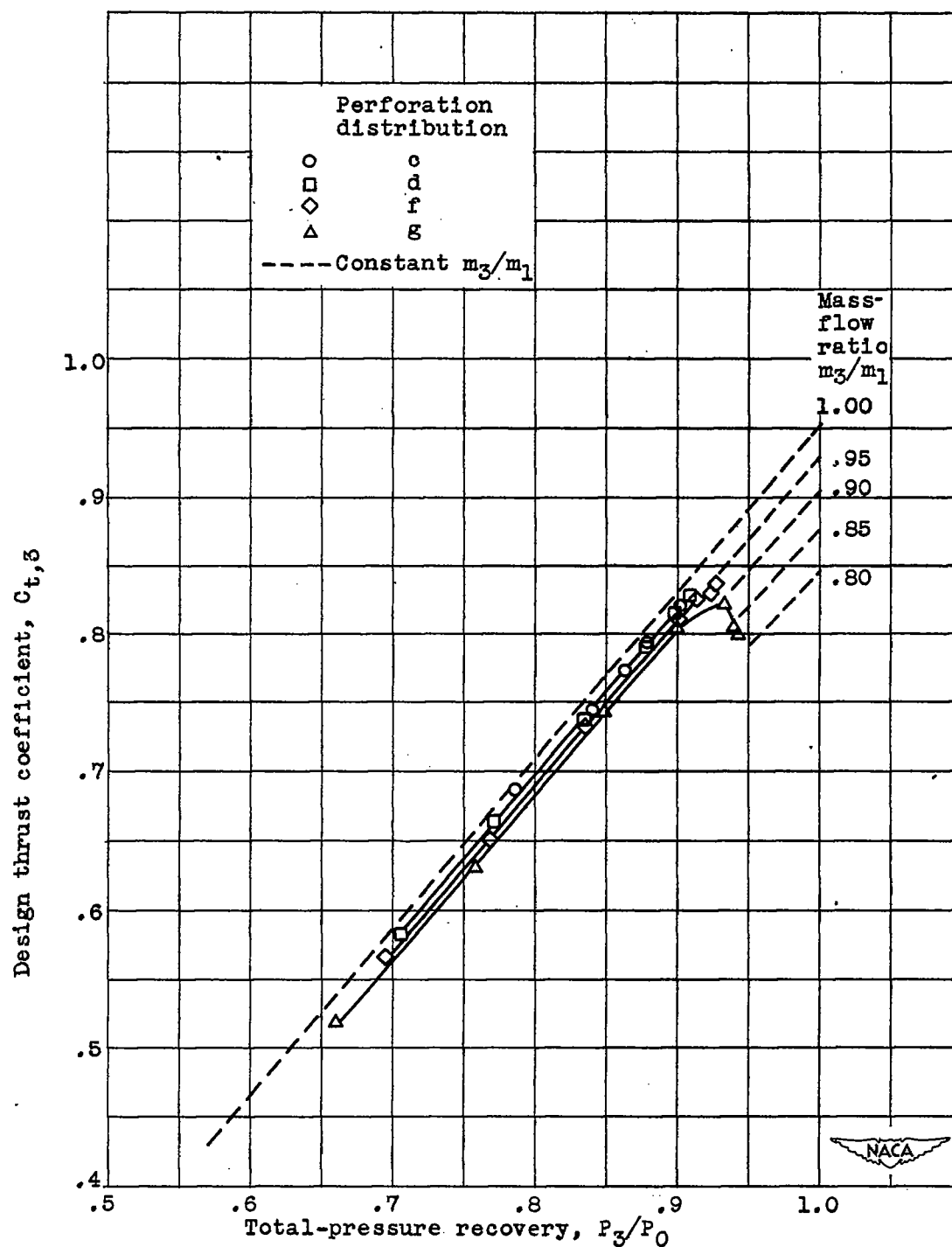


Figure 20. - Thrust coefficient as function of pressure recovery and mass-flow ratio. Contraction ratio, 1.49; free-stream Mach number M_0 , 1.90.



(b) Velocity recovery, 0.6.

Figure 20. - Concluded. Thrust coefficient as function of pressure recovery and mass-flow ratio. Contraction ratio, 1.49; free-stream Mach number M_0 , 1.90.

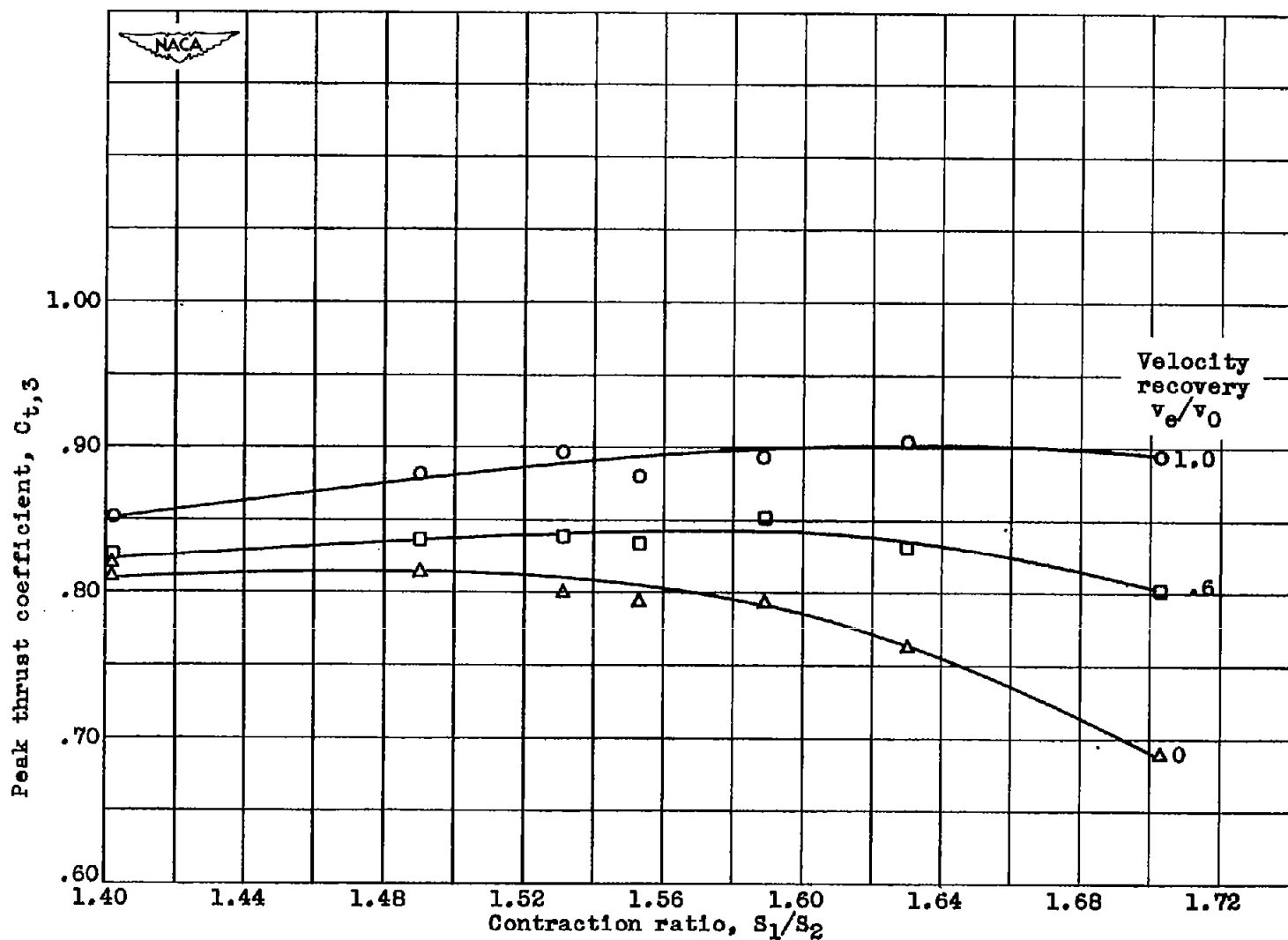


Figure 21. - Peak thrust coefficient as function of contraction ratio for three velocity recoveries.

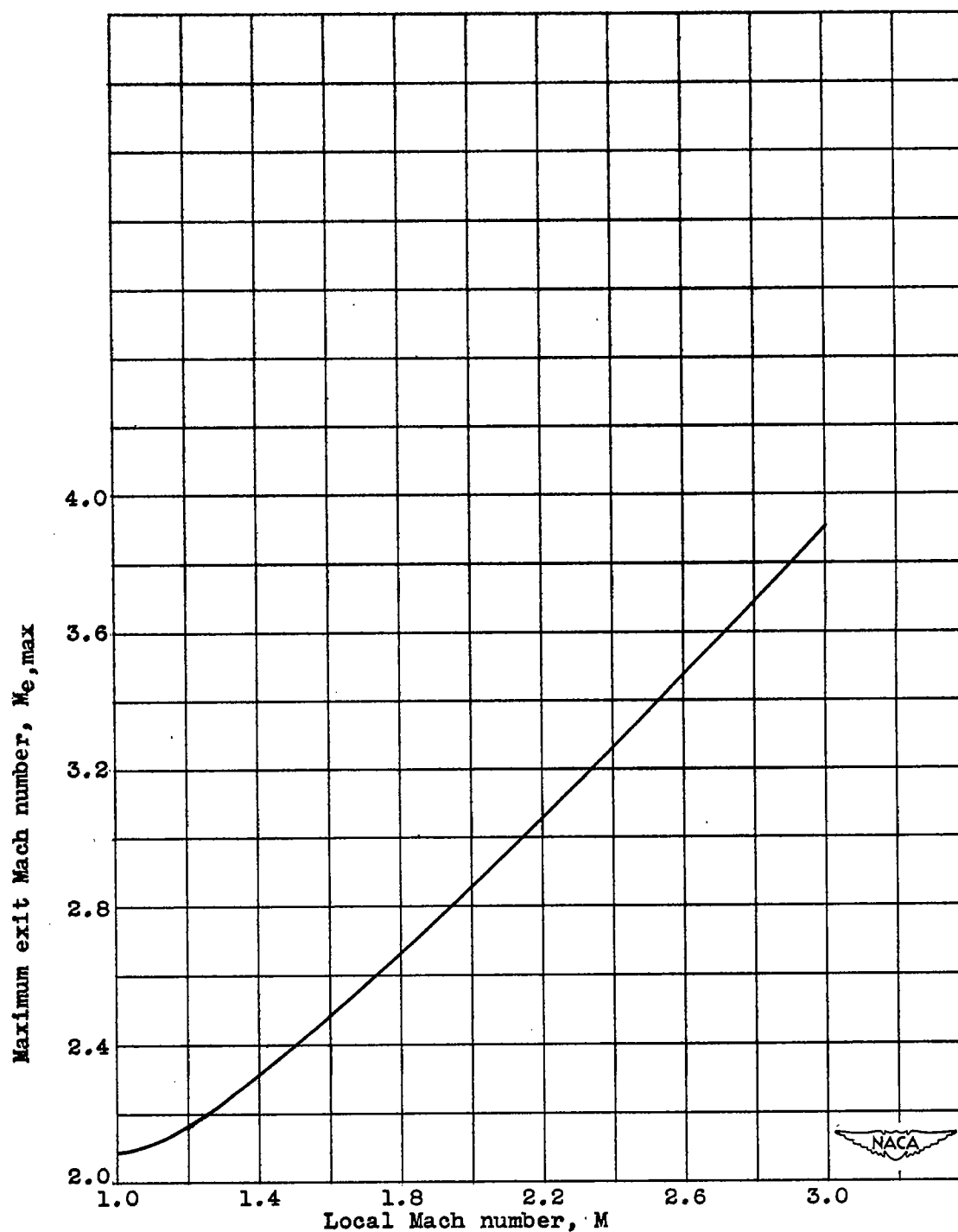


Figure 22. - Exit or critical Mach number as function of local Mach number for perforations in supersonic region of flow.

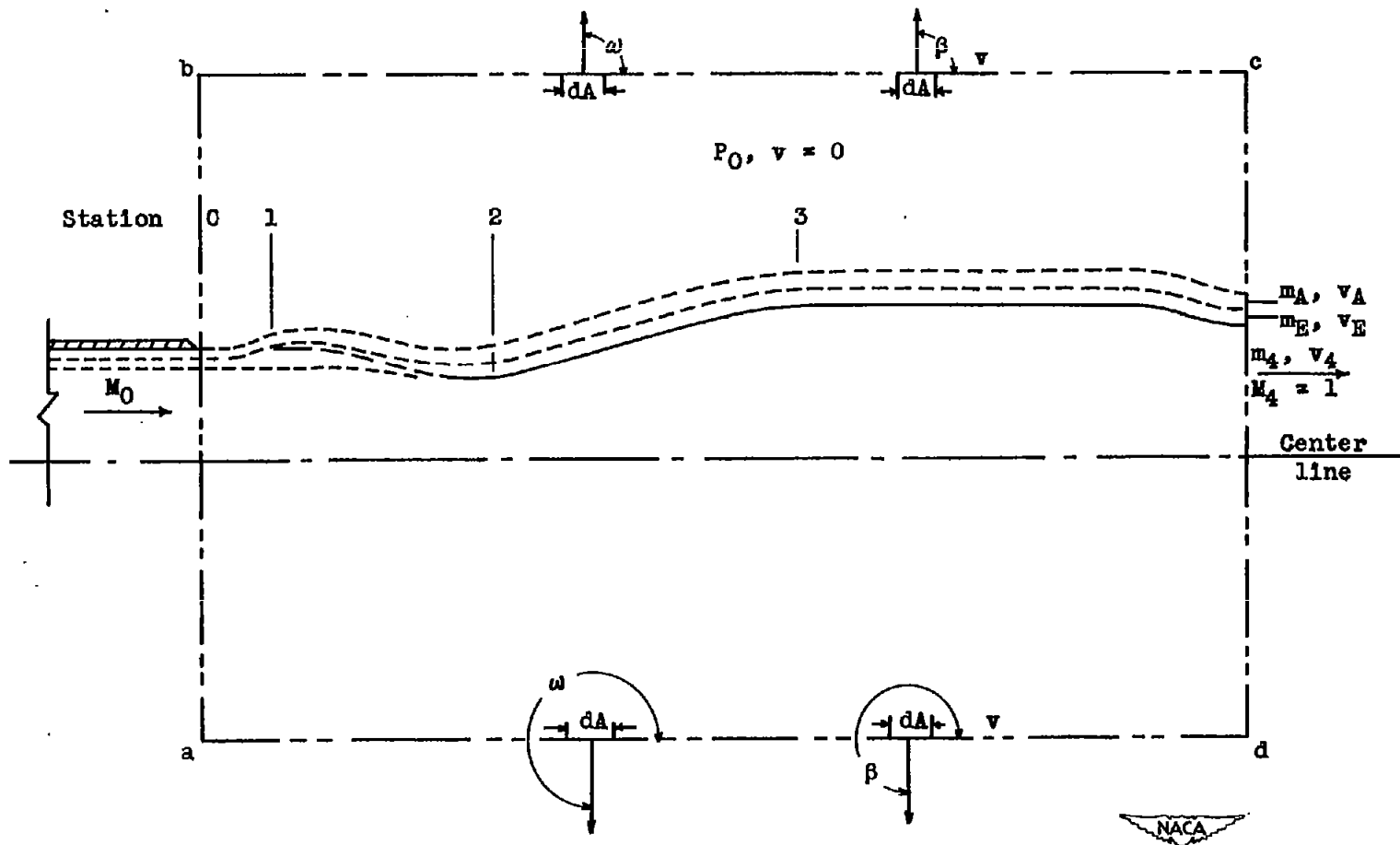


Figure 23. - Schematic arrangement of ram-jet components for derivation of internal thrust.